

1 Addition of brackish water to tundra soils does not inhibit 2 methane production: implications for Arctic coastal methane 3 production

4 **Alexie Roy-Lafontaine**^{1, 5}, Rebecca Lee², Peter M.J. Douglas^{3, 4}, Dustin Whalen², André
5 Pellerin^{1,5}

6 ¹Institut des Sciences de la Mer de Rimouski, Université du Québec à Rimouski, Rimouski, Québec, Canada et Centre
7 de recherche Geotop

8 ²Geological Survey of Canada, Natural Resources Canada, Halifax, Nova Scotia, Canada

9 ³Department of Earth and Planetary Sciences and Geotop Research Centre, McGill University, Montréal, Québec,
10 Canada

11 ⁴Centre d'Études Nordiques, Université Laval, Québec, Québec, Canada

12 ⁵Québec Océan, Université Laval, Québec, Québec, Canada

13 *Correspondence to:* Alexie Roy-Lafontaine (alexieroylafontaine@gmail.com)

14 **Abstract.** In Arctic regions where coastal sediments contain permafrost, global climate change drives processes such
15 as erosion and subsidence. The contribution of these processes to carbon emissions, especially from ground
16 subsidence, are still uncertain. Relative sea level rise can lead to more waterlogged environments, promoting anoxic
17 degradation of organic matter but it can also lead to a greater exposure of coastal sediments to seawater. This could
18 alter methane (CH₄) production dynamics, although the controls remain poorly understood. For instance, sulfates
19 contained in seawater may have a tampering effect on methanogenesis through competitive inhibition but the increase
20 in microbial abundance could enhance methanogenesis. In this study, we present CH₄ production rates alongside
21 geochemical analyses in a rapidly evolving coastal landscape near the community of Tuktoyaktuk, NWT, Canada,
22 which is located in the continuous permafrost zone. To better constrain CH₄ production dynamics along the land to
23 ocean continuum, sediment cores were collected from nearshore marine sediments and soil profiles were collected
24 from the active layer of the coastal (intertidal) zone and inland soils. Anoxic incubations were performed, amended
25 with brackish water to simulate the effect of seawater on the breakdown of organic matter and the production of CH₄.
26 We found marine sediments expectedly led to negligible CH₄ production rates, while the inland sites showed variable
27 rates between null and 35 nmol cm⁻³ d⁻¹. The coastal (intertidal) zone had the highest rates reaching 415 nmol cm⁻³ d⁻¹.
28 Interestingly, sulfate present in brackish water and sediments did not suppress methanogenesis in the incubations of
29 the coastal and inland zones. Analyses of stable carbon isotopes from CH₄ produced in the incubation experiment
30 indicated greater acetotrophy and higher organic matter lability in the coastal zone, possibly contributing to higher
31 CH₄ production rates. This study highlights the potential for significant CH₄ emissions even with high sulfate
32 concentrations which are classically thought to inhibit methanogenesis. This suggests that Arctic coastal microbial
33 CH₄ production might be an understudied source to the atmosphere.

34 **1 Introduction**

35 Arctic coastal ecosystems are impacted by sea level rise, coastal erosion, land submersion, higher frequency in storm
36 events and permafrost degradation (AMAP 2019; Guimond et al., 2021; Irrgang et al., 2022; Lantuit et al., 2013; Lim
37 et al., 2020). The amplification of coastal environmental changes has impacts on biogeochemical cycles (AMAP,
38 2017) and on organic matter (OM) degradation processes and fluxes at the land-ocean continuum (Tanski et al., 2021).
39 Furthermore, the progressive thawing of permafrost exposes long frozen organic matter to microbial decomposition
40 (Lapham et al., 2020; Pellerin et al., 2022; Schuur et al., 2015), leading to the release of greenhouse gases like carbon
41 dioxide (CO₂) and methane (CH₄). Inputs and outputs of the Arctic carbon biogeochemical cycle are known to be
42 reshaped by rapid environmental changes (Couture et al., 2018), but processes in coastal settings are still poorly
43 understood.

44 Rates of coastal change vary according to the morphology of coastal landscapes (Manson et al., 2019). The
45 average rate of land retreat measured in the Tuktoyaktuk Coastlands (North-West Territories, Canada), our study site,
46 between 1985 and 2020 was -1.06 m/yr, while processes of ground subsidence and submersion induced retreat rates
47 higher than -4 m/yr (Costa, 2022) which can inundate large swaths of land. Inundated tundra flats and polygons are
48 widespread landforms in the landscape (Costa, 2022). Polygon tundra flats are characterized by ice-wedge polygons,
49 which are formed by the repeated thermal contraction and expansion of the upper layers of the permafrost (Steedman
50 et al., 2016). At the surface, the polygons are expressed as minor topographic features separated by lower-lying, often
51 wet or inundated channels called troughs (Fig 1). Polygons can be classified as low-centered (with a low, wet center
52 and raised rims) or as high-centered (with well-drained centers and lower well-drained rims) (Fig 1), exhibiting strong
53 thermal, hydrological and geochemical gradients (Vaughn et al., 2016).

54 During growing season, where atmospheric temperatures allow for active layer to thaw and vegetation to
55 grow, hydrological conditions in polygons play a pivotal role in shaping the pathways of OM decomposition and
56 consequently influence the resulting CO₂ and CH₄ production. Well drained oxic conditions allow microbes to
57 decompose OM rapidly, leading to the production of CO₂ (Jones et al., 2020). Conversely, water saturation restricts
58 oxygen availability, promoting anaerobic respiration and fermentation, inducing both CO₂ and CH₄ production
59 (Lipson et al., 2012; Turetsky et al., 2008). Thus, coastal changes and higher atmospheric temperatures during open-
60 water season can swiftly alter water saturation conditions in polygons, in many cases significantly enhancing
61 fermentation and CH₄ production (Elberling et al., 2013; Holm et al., 2020; Treat et al., 2015).

62 Furthermore, coastal changes can also influence the chemistry of the water within soils, which can affect OM
63 degradation. In anaerobic conditions, OM degradation processes follow a sequence of electron acceptors of decreasing
64 energetic yields with nitrate, manganese oxides, iron oxides and sulfate as the most abundant electron acceptors
65 (Froelich et al., 1979). It is when all alternative electron acceptors are depleted that fermentation takes place, leading
66 to the production of CH₄; methanogenesis. For example, it has long been established that in beach, estuarine, and
67 marsh mudflats on the Brittany coast (France), organic matter (OM) degradation is dominated by sulfate reduction, as
68 the high sulfate content of seawater inhibits methanogenesis through competitive inhibition (Winfrey and Ward,

69 1983). In contrast, sediments beneath thermokarst lakes are anoxic and largely devoid of alternative electron acceptors,
70 so OM degradation is almost entirely driven by methanogenesis (Sepulveda-Jauregui et al., 2015). These examples
71 highlight that the chemical composition of the aqueous environment plays a critical role in controlling the pathways
72 of OM degradation. CH₄ produced in soils or sediments can also be oxidized by anaerobic methanotrophic archaea
73 and sulfate-reducing bacteria (Boetius et al., 2000; La et al., 2022) present in the soils or sediment, contributing to
74 lower CH₄ emissions in coastal environments. Thus, on or near the coast, the interaction with seawater, which contains
75 electron acceptors such as sulfate, can shift the OM mineralization pathway and the resulting CO₂ and CH₄
76 productions. Consequently, a nuanced understanding of biogeochemical processes and their drivers is paramount in
77 determining the magnitude of permafrost carbon emissions, especially from coastal environments.

78 Numerous CH₄ emissions monitoring programs are in operation, but remote-sensing methods lack the ability
79 to comprehensively capture the microbial, biogeochemical and environmental processes involved. In specific regions,
80 estimates of methane production from the breakdown of OM is possible by carefully studying degradation pathways
81 and production rates (Pellerin et al., 2022; Heslop et al., 2015; Knoblauch et al., 2018; Treat et al., 2014). To reduce
82 the knowledge gap of CH₄ biogeochemistry in coastal permafrost settings, we collected material from the active layer
83 and taliks of water bodies for incubation experiments, which were coupled to physical and chemical characterizations.
84 The main objective of this study was to assess microbial CH₄ production dynamics in a coastal permafrost setting and
85 apply it at the landscape level, since methane production is well documented in inland thermokarst but is not well
86 understood in a land-ocean interaction context. We hypothesized that methanogenesis in coastal active layer
87 incubations would be suppressed by the addition of sulfate. Consequently, we discuss the influence of environmental
88 conditions on microbial CH₄ production with an emphasis on brackish water addition in coastal soils and sediments
89 along with the microbial pathways involved. We then apply these results at the landscape level to provide an estimate
90 of CH₄ production in the event that a natural process like a storm inputs brackish water over a large area of polygonal
91 patterned ground. We use the region around Tuktoyaktuk as an example.

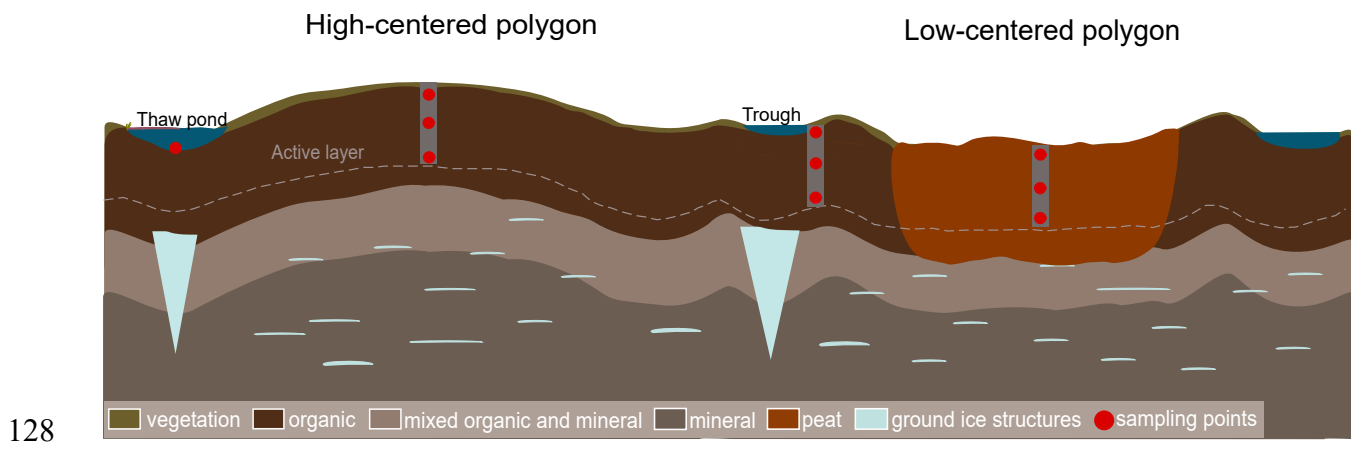
92 **2 Methods**

93 **2.1 Site description and sampling**

94 Tuktoyaktuk (69°26'24'' N, 133°01'52''W) is located in the Inuvik region of the North-West Territories,
95 adjacent to the Arctic Ocean in the Kugmallit Bay, east of the Mackenzie Delta. The region experiences prolonged
96 cold winters, short cool summers, and year-round low precipitation, fostering low-arctic tundra vegetation. Lying in
97 the continuous permafrost zone, its coastal areas feature thick Quaternary and glaciogenic unconsolidated deposits
98 (Rampton, 1988), where permafrost thickness averages 400 m (Hu et al., 2013) and is characterized by prevalent
99 ground ice structures (Mackay and Dallimore, 1992; Martin et al., 2018; Murton, 1996; Rampton, 1988). The area
100 has been ice-free for the past 13 000 years, with evidence indicating that early Holocene summer temperatures were
101 up to 6°C warmer than today, fostering vegetation and peat accumulation (Dallimore et al., 1997; Vardy et al., 1997).
102 During that same period, sea level was considerably lower than it is today and the Tuktoyaktuk area was located
103 approximately 100 km inland (Vardy et al., 1997). Currently, ground subsidence and coastal erosion are major causes

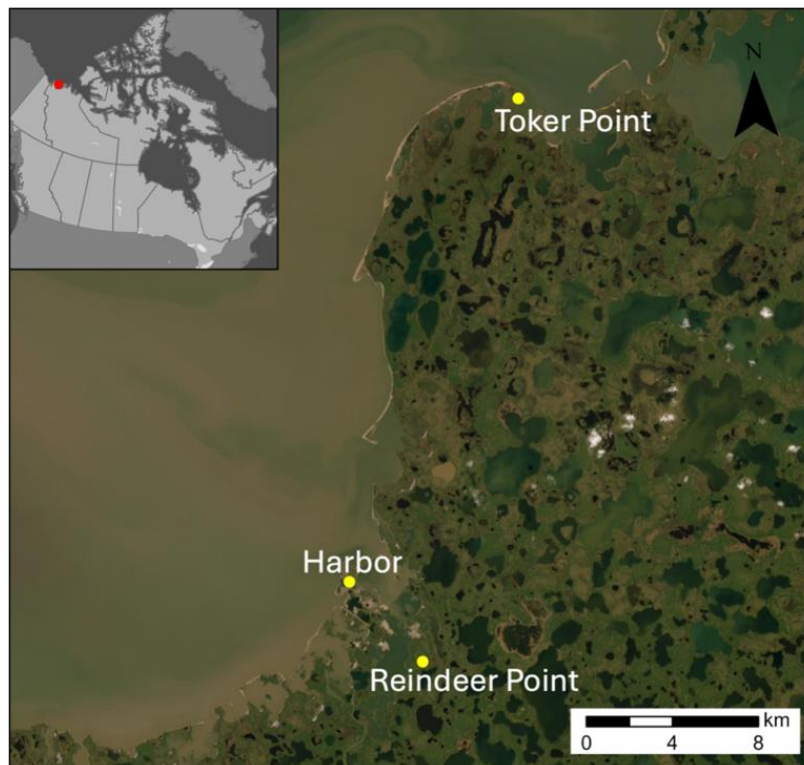
104 of rapid land retreat (Hynes et al., 2014; Lapham et al., 2020; Lim et al., 2020). Combined with sea level rise (Hill et
105 al, 1993), it is projected that a substantial amount of terrestrial soil will become part of the ocean seafloor either by
106 erosion and deposition or by subsidence of land and submersion. Over the past 15 years, extensive studies on
107 Tuktoyaktuk’s coastal environment, driven by the region’s vulnerability to climate change, highlighted challenges for
108 the Inuvialuit population relying on hunting, fishing, trapping and harvesting (Andrachuk and Smit, 2012).

109 Active layer samples were collected from two sites: an inland site, Reindeer Point (RP) and a coastal site, Toker Point
110 (TP). Talik sediments were also collected at both RP and TP sites from polygonal troughs and pondlets and sediments
111 from a marine site, Harbor, completed the transect from terrestrial to marine settings. RP was selected as the inland
112 site because it features a polygonal patterned ground typical of the region, and is located in a stable region not directly
113 affected by coastal processes such as storm surges, tides, seawater intrusion, erosion etc. The thermokarst lake margin,
114 about 300m south of RP has remain unchanged since aerial photos began recording the evolution of the landscape in
115 1947 (Fig S1). TP was selected as the coastal site because of the strong coastal processes such as tides and storm surge
116 that regularly lead to seawater intrusion in this polygonal patterned ground, strongly influenced by ground subsidence.
117 The Harbor site was selected about 400 m offshore in the Harbor of Tuktoyaktuk where total water depth was 20 m
118 and cold marine bottom waters were overlain by a 10 m surface brackish water layer. 25 cm sediment cores were
119 collected using a UWITEC gravity corer. The sediments consisted of recently deposited silty sands originating from
120 the strong erosional processes occurring in the region (Whalen et al., 2022). The site was accessible by small
121 watercraft. At RP and TP sites, soil profiles were extracted from the active layer by digging a soil pit with a shovel.
122 To retain an intact stratigraphic relationship, samples were taken from the wall of the soil pit. Biogenic ebullition
123 gases were collected from pondlets at RP and TP. Pondlets were located within sampled polygonal patterned ground
124 and are defined as small (1 to 3 m²) and shallow standing bodies of water, potentially draining seasonally. Samples
125 were trapped using a plastic funnel attached to a 20 mL glass vial. Surface soil lying at the bottom of the pondlets
126 (Fig. 1) were poked until the vial was filled with gas. Once full, vials were crimped with 20 mm butyl rubber stoppers
127 and aluminum caps. Samples were kept frozen until the time of analyses.



129 **Figure 1.** Schematic representation of polygonal tundra with peat accumulation as seen in continuous permafrost
130 environments and sampling design for this study. High-centered polygons are associated with drier conditions, while
131 low-centered polygons, troughs and pondlets are associated with humid or water-saturated conditions. Vegetation
132 cover and OM reflect the hydrology of sites. Not to scale.

133



134

135 **Figure 2.** Map of study area indicating the sampled sites with yellow dots (ESRI, 2022). Harbor site is located in the
136 marine waters of Tuktoyaktuk, Toker Point site is located in the coastal (intertidal) zone and Reindeer Point site is
137 located inland. High resolution satellite imagery and pictures of soil profiles for RP and TP sites available in
138 supplementary materials (Fig. S3).

139

140 The inland site, (RP), was located 750 m from the coast and 2 km East of Tuktoyaktuk in a polygonal
141 patterned ground. This patterned ground is located in a depression, surrounded by elevated plateaus with observable
142 ground water flowing into the valley. In this area, low-centered polygons exhibited higher moisture levels compared
143 to high-centered polygons. High-centered polygons were colonized by shrubs and small flowering plants like
144 *Ericaceae*, while low-centered polygons were dominated by hydrophilic plants such as grasses and sedges. Wet
145 troughs delimited the polygons, with vegetation reflecting waterlogged conditions. The mean active layer and talik
146 thickness across RP was about 35 cm. Profile 10A was collected from a trough and presented water-saturated
147 conditions with brown OM. Profiles 10B and 10D were collected from high-centered polygons and characterized by
148 unsaturated conditions with dark brown OM and presence of roots until 20 cm depth. Profile 10C was collected from

149 a low-centered polygon and consisted of reddish-brown peat throughout. Profiles 10A, 10B and 10D did not consist
150 of peat.

151 The coastal site (TP) is located 20 km NW of Tuktoyaktuk, featuring a polygonal patterned ground, largely
152 colonized by *Carex sp.*, a type of graminoid plant common near Arctic coastlines. The mean active layer and talik
153 depths were 35 cm. The site's dynamics are influenced by the twice-daily ebb and flow of tides. Profile 07 was
154 collected from a water-saturated low-centered polygon, located in the intertidal zone. The soil color was very dark
155 greyish black. Profile 08 was collected from a water-saturated polygonal trough not immediately located in the
156 intertidal zone, but which floods during storms. The soil was characterized by dark greyish-brown OM mixed with
157 sand. Finally, profile 09, was collected from the center of a higher-centered polygon situated in the middle intertidal
158 zone. The active layer appeared water unsaturated. The soil from this site consisted of a mixture of black organic-rich
159 material and sand. The sand found in samples from TP appeared to be wind-deposited from nearby dunes.

160 **2.2 Sulfates and chloride concentrations in sediments**

161 The extraction of sulfate and chloride from sediments and soils pore-water was conducted through a leaching
162 experiment following Lacelle (2019). Frozen aliquots of sediments and soils were thawed at 4°C overnight, then
163 weighed, dried in the oven at 60°C for 24 hours and re-weighed to determine the densities. Aliquots of dried material
164 were put in 50 mL falcon tubes with nanopure water following a 1:10 ratio. Tubes were then shaken for one hour to
165 promote leaching of anions towards the aqueous phase of the solution. Once the leaching process was done, 2 mL of
166 the aqueous solution was filtered using 0.2 µm pore size Whatman 25 mm GD/X syringe filters and transferred in
167 disposable microtubes. Concentrations of sulfate and chloride were measured by ion chromatography using a Thermo
168 Dionex Integriion at UQAR's Chemistry department facilities with a limit of detection of 0,01 µg/mL. The measured
169 concentrations are expressed in mmol g⁻¹ wet-weight⁻¹ of material (mmol g⁻¹ wweight⁻¹). Only one measurement per
170 sample was performed as stability tests revealed variability of less than 3% between measured samples. The error on
171 each value was calculated by the least squares method (Skoog et al., 2014).

172 **2.3 Methane production rates in incubations**

173 Long-term sediment and soil incubations under anoxic conditions were used to assess CH₄ production rates
174 over several months by measuring CH₄ accumulation in the vials' headspace. The objective was to simulate the
175 increased connectivity between the land and the ocean in the coastal environment of the Canadian Arctic, which
176 represents an important aspect of the ongoing regional environmental transition. Collected sediments and soil profiles
177 were immediately sub-sampled based on depth, at 5 or 10 cm intervals, according to shifts in sedimentary units. To
178 prepare incubations, about 4 mL of sediment and exactly 2 mL of brackish water (collected from the coast) were
179 immediately transferred into 20 mL glass vials. Incubation vials were crimped with 20 mm blue chlorobutyl rubber
180 stoppers and aluminum caps. The bottles were flushed with nitrogen gas (Alpha Gaz 1) at a rate of 300mL/min for 2
181 minutes in the field to replace the air with a nitrogen atmosphere. Four incubations were prepared for each sampled
182 depth; 3 were kept for measurements of CH₄ production rates (triplicates) and one served for isotopic analyses.
183 Incubations were kept at a constant temperature of 4°C throughout the entire 339 days incubation period with no

184 fluctuations. Substrate concentrations were not actively controlled or monitored, aside from repeated measurements
185 of headspace methane. CH₄ accumulation was measured bimonthly from day 227 until day 339. The brackish
186 water added to all incubations contained $5.7 \pm 0.0 \text{ mmol g}^{-1} \text{ wweight}^{-1}$ of sulfate and $28.7 \pm 0.5 \text{ mmol g}^{-1} \text{ wweight}^{-1}$
187 of chloride.

188 Analyses of the CH₄ concentrations in the headspace of the vials were performed on a gas chromatograph
189 (Agilent 8900) equipped with a flame ionization detector (GC-FID) at UQAR facilities. The GC-FID is equipped with
190 a 100 μL injection loop to ensure a consistent volume of sample is analyzed. To saturate the injection loop, 300 μL
191 are taken from the headspace of the vials and transferred to the injection loop with a gas-tight syringe. Prior to
192 injection, samples were shaken for 30 seconds to equilibrate headspace and sediment gases. This procedure was done
193 for 16 weeks to measure CH₄ accumulation in the headspace. The resulting production rates were calculated from the
194 CH₄ accumulation measured during the incubation period. The whole measurement interval was retained regardless
195 of CH₄ concentration dynamics to avoid selective exclusion. Rates were derived from the slope of concentration
196 change over time and are expressed in $\text{nmol cm}^{-3} \text{ d}^{-1}$ and the standard deviation from triplicate incubation was reported
197 as the uncertainty estimate. The density of the collected samples varied widely, with some being organic deposits and
198 peat, while others contained higher mineral content. Consequently, the CH₄ production rates were expressed
199 volumetrically to account for these discrepancies which are more representative of the volume they occupy in the soil,
200 sedimentary columns and landscape. The limit of detection of the GC-FID is 0.3 ppm and all samples had higher
201 concentrations. Each value represents the mean of triplicate measurements and the reported uncertainty on the
202 measurement is the standard deviation on triplicates.

203 To estimate the potential total active layer CH₄ production (T), the active layer production rates were
204 vertically integrated to obtain the total CH₄ production of each profile. Values are reported in $\text{mmol m}^{-2} \text{ d}^{-1}$ and were
205 calculated using eq. 1:

$$206 \quad T = \frac{1}{100} \sum_{i=1}^n P_i \cdot e_i \quad [\text{mmol m}^{-2} \text{ d}^{-1}] \quad \text{eq. 1}$$

207 Where P_i represents CH₄ production rate in layer i ($\text{nmol cm}^{-3} \text{ d}^{-1}$), e_i represents the thickness of layer i (cm)
208 and n represents the numbers of layers in the profile.

209 Using aerial imagery from 2022, the polygonal tundra at RP was mapped in QGIS, allowing for the
210 discrimination between high-centered polygons, low-centered polygons and throughs (Fig S2). The total area of each
211 geomorphological form was calculated based on the map data (Table S1). Landforms total areas were multiplied by
212 the corresponding potential total active layer methane production (T) to estimate the total CH₄ produced in the
213 polygonal tundra of RP over a day (mol d^{-1}).

214 **2.4 Elemental and isotope composition of the sediment**

215 The total organic carbon (TOC) content of the sediments was measured by combustion using an elemental
216 analyzer (ECS 8020, NC Technologies) combined with a gas chromatograph equipped with a thermal conductivity

217 detector at ULaval facilities (The International Research Laboratory Takuvik). A 100 mg aliquot of sediment was
218 thawed and weighed for each sample. They were then dried in an oven at 60°C for 48 hours and re-weighed to
219 determine their water content. Sediments were then ground using a granite mortar pestle and homogenized using a
220 1.18 mm pore size sieve to remove roots and rootlets. Instruments were cleaned with ethanol between manipulations.
221 Inorganic carbon was removed from sediments by adding 2.2 mL of 12M HCl in every sample. After reacting for 24
222 hours, around 8 mg was encapsulated in tin foil capsules. Samples were kept in a desiccator until analyses. Values are
223 expressed as % of carbon contained in the weighed sample (wt. %).

224 The organic carbon ($\delta^{13}\text{C}$ -TOC) isotopic compositions were measured at UOttawa facilities (Jàn Veizer
225 Stable Isotope Laboratory) using EA-IRMS (Delta Advantage, Thermo Germany). The sample preparation method
226 was the same used for elemental analyses. $\delta^{13}\text{C}$ -TOC values are denoted as $\delta\text{‰} = 10^3 \left(\frac{R_{\text{sample}}}{R_{\text{standard}}} - 1 \right)$, where R is
227 $^{13}\text{C}/^{12}\text{C}$ and standards refer to the Vienna Pee Dee Belmnite (VPDP).

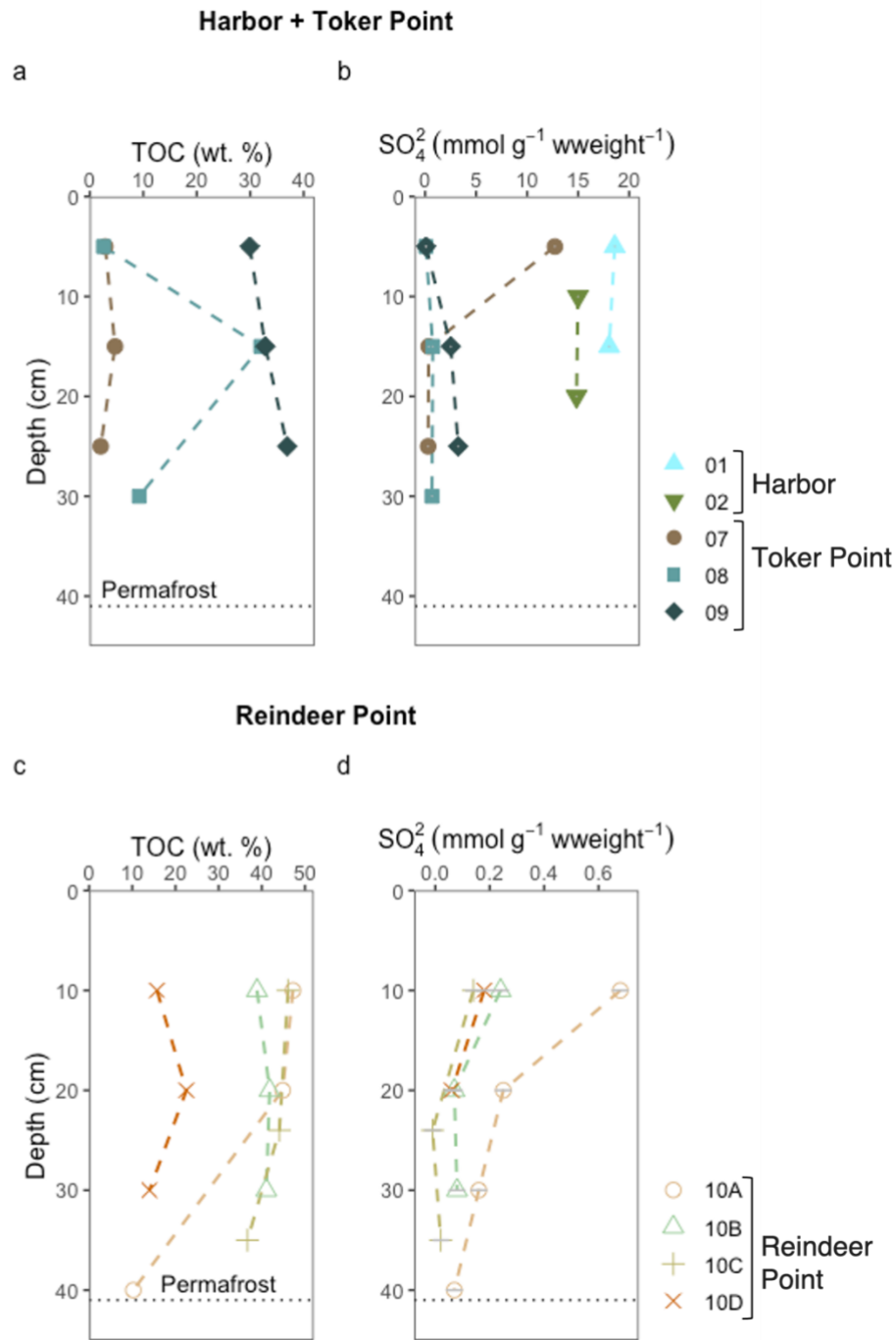
228 **2.5 Stable carbon isotopic composition of methane**

229 One incubation vial was analyzed for stable carbon isotopic composition of headspace methane ($\delta^{13}\text{C}$ -CH₄).
230 Stable carbon from methane ebullition samples collected from pondlets were also analyzed. Both types of samples
231 were analyzed with a cavity ring-down spectrometer (PICARRO G2201-i isotopic CO₂/CH₄) equipped with a 16-port
232 distribution manifold and small sample introduction module (SSIM) at McGill (McGill Isotope Biogeochemistry
233 Laboratory). Incubations were kept at 4°C in the dark for 8 months to let the microbial community stabilize and
234 produce sufficient CH₄ for analysis. To stay in the detection range of the analyzer (1.8-1000 ppm CH₄), a small volume
235 of the headspace, proportional to CH₄ concentration in sample, was drawn from the incubation vial (0.2-6 mL). The
236 sample was introduced to the 16-port manifold with a 21G needle connected to a disposable luer lock plastic syringe.
237 Samples were diluted with zero air by the SSIM to reach a volume of 20 mL. Two or three measurements per sample
238 were conducted depending on headspace concentration. Ebullition gases samples were analyzed following the same
239 method. Measured values were corrected with internal certified methane standards (-59 ‰ and -42‰) from AirLiquide
240 and stability of the analyzer was tested with injections of ambient air. Measured values were more precise than \pm
241 1.2‰. All $\delta^{13}\text{C}$ -CH₄ values are expressed relatively to VPDB. While those isotopic analyses results provide valuable
242 insight into methane cycling processes, they should be interpreted with caution in the absence of biological replication.

243 **3 Results**

244 **3.1 Soil description and composition**

245 TOC content in the sampled soils ranged from 2 to 47 wt. %, with no clear trend in relation to depth (Fig 3,
246 a, c). The RP polygonal patterned ground featured organic soils with TOC content ranging from 14 to 47 wt. % (Fig
247 3, c). The TP coastal polygonal patterned ground also featured organic soils with TOC content ranging from 2 to 37
248 wt. % (Fig 3, a).



249

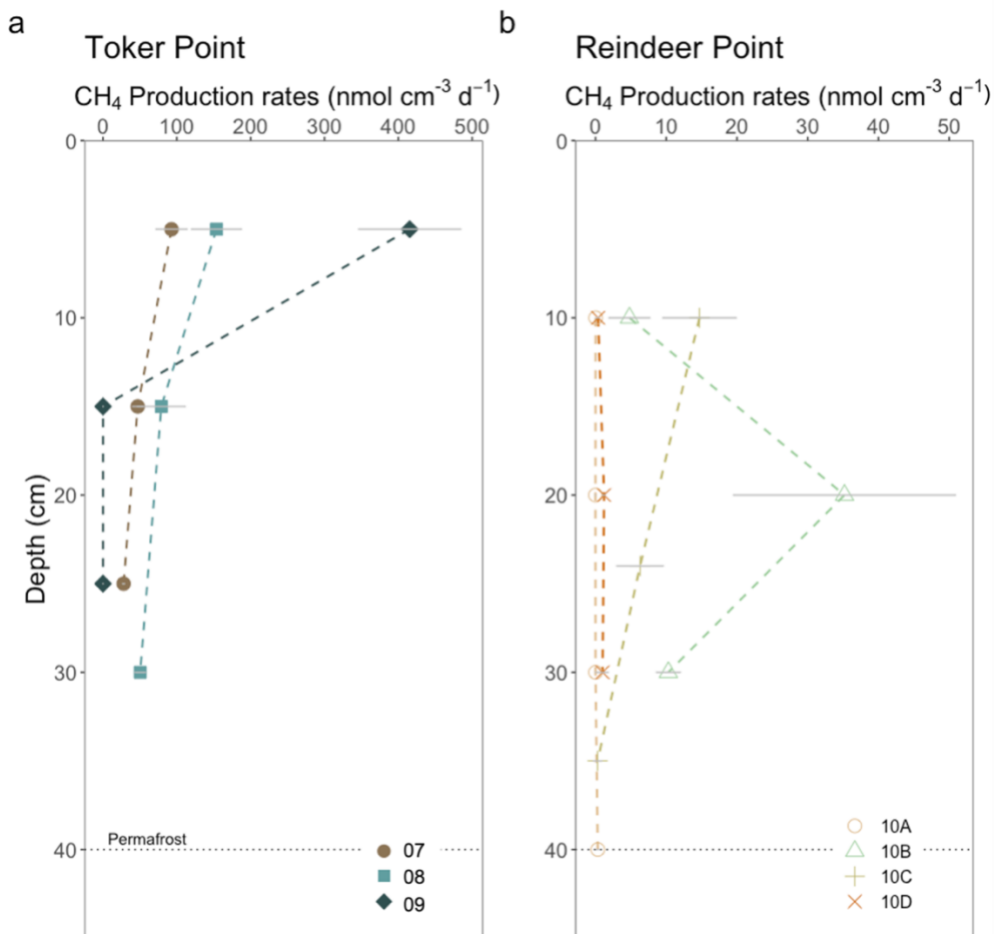
250 **Figure 3.** Total organic carbon and sulfate (SO_4^{2-}) concentrations in sediment or soil of different sites in this study.
 251 The datasets are separated into two for clarity. The upper part of the figure (panels A and B) displays the data of the
 252 marine site Harbor (profile 01 and 02), and the coastal site, Toker Point (profile 07, 08 and 09). The lower part of the
 253 figure (panel C and D) displays the data from the inland site Reindeer Point (profile 10A, 10B, 10C and 10D). The
 254 black horizontal dotted line in each graph represents the permafrost-active layer or talik interface except for the Harbor

255 site, where the talik is much deeper but not measured. TOC data from Harbor site is not available. A uniform color
256 pattern is used throughout this manuscript.

257 RP, the inland site, had low sulfate and chloride concentrations relative to TP, the coastal site (Fig 3 (b), (d)
258 and S2). Sulfates at RP ranged from null concentrations to $0.68 \pm 0.03 \text{ mmol g}^{-1} \text{ wweight}^{-1}$, while at TP, profiles
259 exhibited varying concentrations and patterns in relation to depth. Sulfate concentrations, ranged from 0.07 ± 0.03 to
260 $12.72 \pm 0.03 \text{ mmol g}^{-1} \text{ wweight}^{-1}$. Profile 07, the low-centered polygon, exhibited the highest sulfates concentrations
261 of all TP site at its surface ($12.72 \pm 0.03 \text{ mmol g}^{-1} \text{ wweight}^{-1}$), with concentrations decreasing drastically with depth,
262 reaching $0.29 \pm 0.03 \text{ mmol g}^{-1} \text{ wweight}^{-1}$ at 25 cm (Fig 3, a). In profile 09, the high-centered polygon, sulfate
263 concentrations increased with depth ranging from $0.09 \pm 0.03 \text{ mmol g}^{-1} \text{ wweight}^{-1}$ at 5 cm to $3.2 \pm 0.03 \text{ mmol g}^{-1}$
264 wweight^{-1} at 25 cm. Finally, profile 08, characterized as a polygonal trough, had sulfate concentrations ranging from
265 0.07 ± 0.03 to $0.75 \pm 0.03 \text{ mmol g}^{-1} \text{ wweight}^{-1}$. The highest sulfate concentrations measured in this study were found
266 in the sediments of the Harbor site, with a mean value of $16.6 \text{ mmol g}^{-1} \text{ wweight}^{-1}$ (Fig 3, a).

267 3.2 Methane production

268 Rates of CH_4 production in incubations of sediment and soil with brackish water were undertaken at the three
269 studied sites: RP, TP and Harbor. Production rates ranged from null to $415.4 \pm 69.2 \text{ nmol cm}^{-3} \text{ d}^{-1}$ (Fig 4) throughout
270 all samples in this study. At RP, the maximum CH_4 production rate of $35.2 \pm 15.7 \text{ nmol cm}^{-3} \text{ d}^{-1}$ was measured in the
271 trough profile (10B) at a depth of 20 cm. Lower values were obtained for the surface and at the talik-permafrost
272 interface. The low-centered polygon (10C) had its maximum CH_4 production rate in the surface, decreasing with
273 depth. High-centered polygons (10A and 10D) had very low production rates along their depth profiles ranging
274 between null to $1.2 \pm 0.2 \text{ nmol cm}^{-3} \text{ d}^{-1}$. Both water-saturated trough and low-centered polygon (10B,10C) had
275 relatively high CH_4 production rate compared with the high-centered polygon profiles (10A, 10D), which were water-
276 unsaturated.

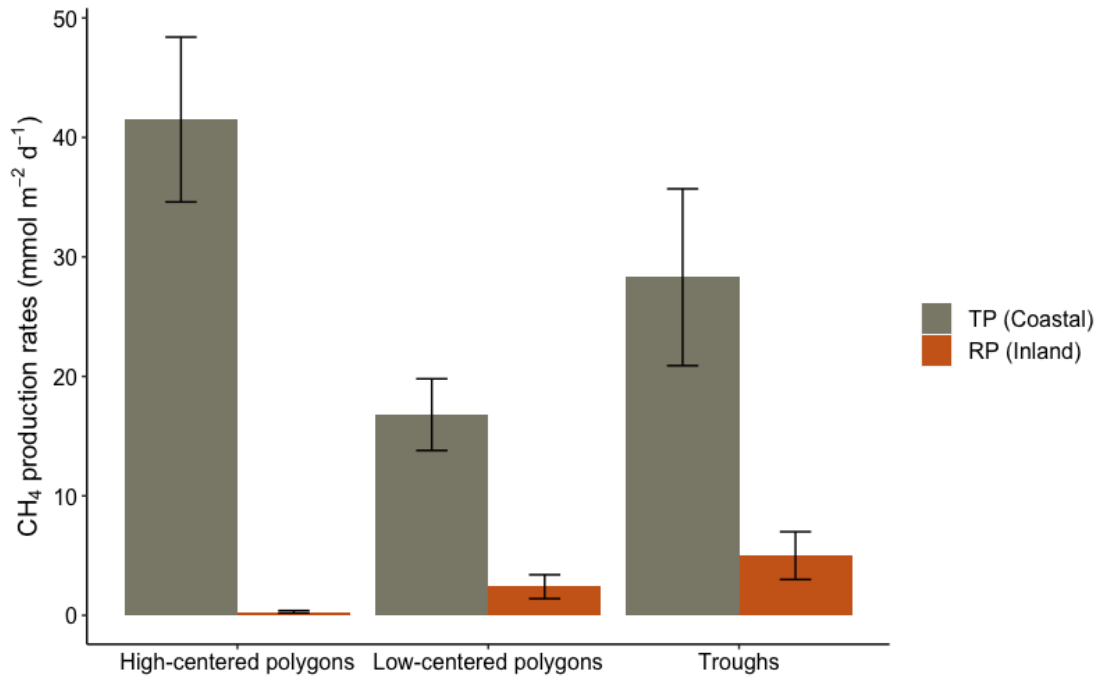


277

278 **Figure 4.** CH₄ production in incubations of soil and sediment with brackish water from (a) TP and (b) RP. Each
 279 datapoint represent the mean value of three incubations. The error bars in grey lines are equal to the standard deviation
 280 of the three separate incubations. Each profile corresponds to a specific landform. At Toker Point (panel A), profile
 281 07 is from a low-centered polygon, profile 08 is from a trough and profile 09 is from a high-centered polygon. At
 282 Reindeer point (panel B), profile 10A is from a high-centered polygon, profile 10B is from a trough, profile 10C is
 283 from a low-centered polygon and profile 10D is from a high-centered polygon.

284 At TP, a maximum CH₄ production rate was recorded in profile 09, the high-centered polygon at $415.4 \pm$
 285 $69.2 \text{ nmol cm}^{-3} \text{ d}^{-1}$ at the uppermost depth but it quickly decreased in the subsurface. Profile 08, the trough, and profile
 286 07, the low-centered polygon, had lower sub-surface CH₄ production rates, but rates decreased less drastically with
 287 depth with values being relatively high at the permafrost-talik and permafrost-active layer interface, respectively.
 288 Profile 07 had values ranging from $27.9 \pm 1.5 \text{ nmol cm}^{-3} \text{ d}^{-1}$ to $92.8 \pm 21.2 \text{ nmol cm}^{-3} \text{ d}^{-1}$ and profile 08 had values
 289 ranging from $50.4 \pm 7.2 \text{ nmol cm}^{-3} \text{ d}^{-1}$ and $153.7 \pm 33.9 \text{ nmol cm}^{-3} \text{ d}^{-1}$ (Fig 4). In general, at TP, the coastal site, much
 290 higher CH₄ production rates were measured than at RP, the inland site (Fig 4). The mean CH₄ production rate measured
 291 at RP was $5.7 \text{ nmol cm}^{-3} \text{ d}^{-1}$, while at TP it was $96.2 \text{ nmol cm}^{-3} \text{ d}^{-1}$. The incubations with silty-clay Harbor sediments
 292 did not have measurable CH₄ production rates (Fig S5).

293 Estimated total CH₄ production rates were calculated for each geomorphological landforms of RP and TP
 294 sites. At RP, the total CH₄ production estimated for the high-centered polygons (profile 10A and 10D), low-centered
 295 polygon (profile 10C) and trough (profile 10B) were $0.3 \pm 0.1 \text{ mmol m}^{-2} \text{ d}^{-1}$, $2.4 \pm 1.0 \text{ mmol m}^{-2} \text{ d}^{-1}$ and $5 \pm 2 \text{ mmol}$
 296 $\text{m}^{-2} \text{ d}^{-1}$, respectively (Fig 5). At TP, the total CH₄ production estimated for the high-centered polygon (profile 09), the
 297 low-centered polygon (profile 07) and the through (profile 08) were $41.5 \pm 6.9 \text{ mmol m}^{-2} \text{ d}^{-1}$, $16.8 \pm 3.0 \text{ mmol m}^{-2} \text{ d}^{-1}$
 298 and $28.3 \pm 7.4 \text{ mmol m}^{-2} \text{ d}^{-1}$, respectively (Fig 5). In all landforms, the total CH₄ production rates were higher in the
 299 coastal site, TP, than the inland site, RP.

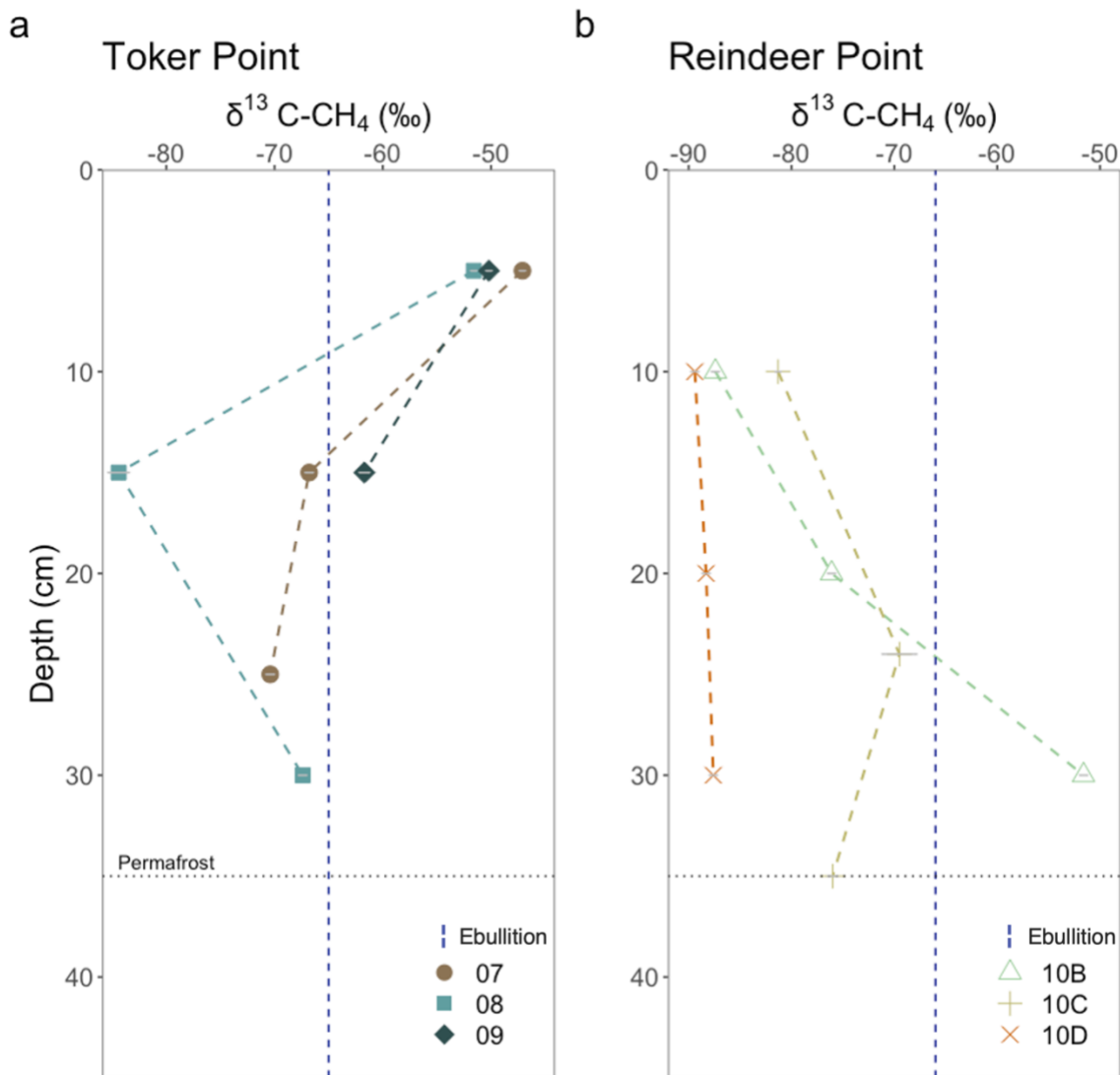


300

301 **Figure 5.** Total CH₄ production rates (T) at Toker Point (Coastal) and Reindeer Point (Inland) organized by
 302 geomorphological forms of high-centered polygons, low-centered polygons and troughs. High-centered polygons at
 303 RP is the mean of two profiles. All other landforms at RP and TP are one profile. The uncertainty on T is propagated
 304 from the uncertainty of individual CH₄ production rates, not averages from replicate sites.

305 3.3 Isotopic composition of ¹³C-CH₄

306 In parallel with CH₄ production rates, one incubation vial per depth was used to measure the stable carbon
 307 isotopic composition of the CH₄ produced. At RP, the δ¹³C-CH₄ of the first sampled depth (10 cm) ranged from -
 308 81.3‰ to -89.4‰. At TP, the coastal site, the δ¹³C-CH₄ signature of the first sampled depth (5 cm) ranged from -
 309 47.1‰ and -51.6‰. The values cluster together based on site, suggesting surface OM degradation processes are most
 310 similar within sites than between sites (Fig. 6). Profiles at RP became progressively enriched in ¹³C with depth, except
 311 for profile 10C where a more depleted value was observed at 35 cm. Conversely, at TP, profiles became depleted in
 312 ¹³C with depth, except for profile 08 where an enrichment was measured between 15 and 30 cm.



313

314 **Figure 6.** Isotopic composition of CH₄ produced in brackish water incubations from (a) TP and (b) RP. Each datapoint
 315 corresponds to the mean value of two or three measurements done on one incubation, depending on the headspace
 316 concentration. The dashed vertical lines correspond to in situ ebullition CH₄ collected in pondlets at each sampling
 317 site (n=1). These values give information on the pathways used by the soil microbes to produce CH₄. δ¹³C between -
 318 65‰ and -50‰ is typically associated with acetoclastic methanogenesis, while δ¹³C between -110‰ and -60‰ is
 319 associated with hydrogenotrophic methanogenesis (Hornibrook et al., 1997, 2000). The grey error bars on each point
 320 represents the analytical uncertainty on the measured value. If not visible, the uncertainty is smaller than the point.

321 Ebullition samples from pondlets were also measured for stable isotopes. The ebullition samples represent
 322 the net δ¹³C signature of methane produced in the sediments of pondlets at RP and TP. At RP, CH₄ ebullition from a
 323 sampled thaw pond had a δ¹³C of -66.1‰ (fig 6). At TP, CH₄ ebullition from a sampled pondlet had a δ¹³C-CH₄ of -
 324 65.0‰ (fig 6).

325 4 Discussion

326 4.1 Addition of brackish water to anoxic incubations did not strongly suppress methanogenesis

327 Before discussing the effects of brackish water addition in incubation experiments, it is important to clarify the
328 role of sulfate measured in situ within soil and sediment profiles. Across the studied sites, sulfate concentrations varied
329 with depth and between landforms; however, this spatial variability did not show a consistent relationship with
330 methane production rates measured in the incubations (Fig S4). A few layers clearly contained higher sulfate amounts.
331 However, layers characterized by higher or lower sulfate concentrations did not systematically correspond to lower or
332 higher CH₄ production, indicating that in situ sulfate availability alone does not explain the observed patterns in
333 methane production across profiles. This interpretation is subject to important limitations. Sulfate and chloride
334 concentrations were measured at single points within each profile and were not replicated across multiple locations
335 within the same landform, preventing resolution of fine-scale spatial heterogeneity in electron-acceptor availability.
336 As a result, sulfate concentrations are interpreted here as first-order indicators of geochemical context rather than as
337 spatially representative or mechanistic controls on methane production. Given these constraints, we focus the
338 following discussion on the experimental addition of sulfate via brackish water during anoxic incubations, which
339 evaluate how episodic marine influence may affect methane production potential in coastal permafrost environments.

340 Despite the addition of brackish water containing sulfate to incubations, the range of CH₄ production rates
341 measured in this study is consistent with reports for anaerobic incubations of recently thawed permafrost soils,
342 suggesting that the input of brackish water to some coastal systems may not inhibit CH₄ production. For example, in
343 the talik of Big Trail Lake, a young thermokarst lake in the interior of Alaska, CH₄ production rates based on
344 incubations ranged between 4.7 and 16.1 nmol cm⁻³ d⁻¹ (Pellerin et al., 2022), while in incubations from Vault Lake,
345 another thermokarst lake in the interior of Alaska, CH₄ production rates varied between 11.1 and 275 nmol cm⁻³ d⁻¹
346 (Heslop et al., 2015). In active layer incubations from the Yamal Peninsula in NW Siberia (Russia), CH₄ production
347 rates of incubations varied between 0.1 and 33.8 nmol cm⁻³ d⁻¹ (Heyer et al., 2002). This indicates that overall, the
348 CH₄ production rates measured at both TP and RP are within the range observed in typical ice-rich permafrost settings
349 and reasonable for the environment studied (Fig. 4). We note that our experimental design did not include parallel
350 incubations without brackish water or with sulfate concentration gradients; therefore, our interpretation relies in part
351 on comparison with previous incubations of Tuktoyaktuk soils conducted without brackish water addition (Lapham
352 et al., 2020) and should be regarded as exploratory rather than definitive. Lapham et al. (2021) conducted sediment
353 incubation experiments using a core collected from the coast of the Tuktoyaktuk Peninsula. In their study, CH₄
354 production was measured under anaerobic conditions at 15 °C, without the addition of water, over a 35-day period.
355 The reported CH₄ production rate was 0.07 nmol cm⁻³ d⁻¹. Although their incubations were performed over a shorter
356 duration and at a significantly higher temperature than those in the present study, the measured rate reflects CH₄
357 production under relatively natural, unamended conditions. This value is comparable to the lowest CH₄ production
358 rates measured in our incubations at both the coastal (TP) and inland (RP) sites and provides a useful reference for
359 CH₄ production under unamended conditions.

360 The novel aspect of this study is that it attempts to understand marine influence on OM degradation by addition
361 of brackish water to sediment and soil incubations of a fully marine site (Harbor), one that is periodically submerged
362 (TP) and never submerged (RP). This simulates the input of seawater to the active layer and taliks of tundra soils (RP)
363 as well as providing reference sites with a high marine influence (Harbor and TP). We hypothesized that the addition
364 of locally obtained brackish water, which contained sulfate (5.7 mmol L⁻¹), to the incubations, would suppress CH₄
365 production in RP, the inland site and potentially also at TP, the coastal site. This reasoning is because supplying sulfate
366 to low sulfate organic-rich sediment would promote sulfate reduction, which is thermodynamically more favorable
367 than methanogenesis, thereby competitively inhibiting it (Lovely and Klug, 1983; Oremland and Polcin, 1982). This
368 hypothesis is also consistent with field observations; organic matter mineralization in brackish wetlands is consistently
369 dominated by bacterial sulfate reduction (Bridgham et al., 2013; Torres-Alvarado et al., 2005) where little to no
370 CH₄ emissions are observed (Pönisch et al., 2022; Petersen et al., 2023; Kroeger et al., 2017). However, recent field
371 studies show that in coastal permafrost soils, inundation and low sulfate concentrations do not necessarily suppress
372 methanogenesis (Jenrich et al., 2025; Jenrich et al., 2024; Yang et al., 2023). These contrasting observations reveal a
373 key knowledge gap in how marine influence controls carbon mineralization pathways in permafrost systems. By
374 experimentally testing brackish water additions across sites with contrasting marine exposure, our study provides new
375 insights into the regulation of OM degradation and CH₄ production under ongoing Arctic coastal change.

376 RP had low sulfate concentrations before addition of the brackish water but so did many of the profiles from TP
377 (Fig 3). In the Harbor sediments, no methane production was observed (Fig S5). This is consistent with processes
378 typically observed in marine systems, where electron acceptors like oxygen, nitrate, iron oxides or sulfate are
379 associated with low CH₄ production e.g. (Martens and Berner, 1974) as well as the potential for anaerobic oxidation
380 of methane (AOM). Given that the Harbor sediments already had high sulfate concentrations, the lack of methane
381 production with addition of brackish water was expected. However, strong CH₄ production was observed in the
382 incubations of both the coastal site TP and the inland site RP, indicating that CH₄ production occurred despite the
383 addition of sulfate via the brackish water. However, as no incubations without brackish water addition or sulfate
384 gradient experiments were conducted, the extent to which sulfate may have suppressed methanogenesis relative to
385 baseline conditions cannot be assessed. While sulfate reduction rates were not measured and therefore not
386 demonstrated directly in our incubations, a strong sulfide smell was recorded when opening most of the incubations
387 at the end of the experiment. This observation may indicate the coexistence of sulfate reduction and methanogenesis
388 during the incubations. However, to rigorously assess this observation, future studies should include tracer-based
389 sulfate reduction assays and microbial functional gene analysis.

390 Coexistence of sulfate and methanogenesis within complex sediment systems such as estuarine, coastal and salt
391 marsh sediments, as well as thermokarst lasens has been widely reported (Lovely et al., 1982; Oremland and Taylor,
392 1978; Sela-Adler et al., 2017; Yang et al., 2023). Two main mechanisms are invoked to explain the observed CH₄
393 production in the presence of sulfate in our incubation experiment: (1) noncompetitive methanogenesis (i.e.
394 methylotrophic methanogenesis) and (2) syntrophic methanogenesis. (1) Noncompetitive substrates are substrates like
395 methanol and methylamines that are used by methanogens alone and cannot be used with electron acceptors like

396 sulfate (Lovley and Klug, 1983; Oremland et al., 1982). Noncompetitive substrates are thus microbially converted to
397 CH₄, even in sediments with high sulfate concentrations (Maltby et al., 2018; Yuan et al., 2019). For example, in salt
398 marshes, where high sulfate concentrations are often found, elevated CH₄ emissions are suggested to mainly stem
399 from noncompetitive methanogenesis (Comer-Warner et al., 2022; Poffenbarger et al., 2011; Yuan et al., 2019). In
400 the sulfate reducing zone of sediments from the Baltic Sea, where ample sulfate is found in the porewaters, seasonal
401 methanogenesis rates were measured up to 1.3 nmol cm⁻³ d⁻¹ due to noncompetitive substrates (Maltby et al., 2018).
402 In permafrost soils, methanol, methylamines and the microorganisms capable of degrading them have been observed
403 but their concentrations are typically low (Coolen and Orsi, 2015; Kramshoj et al., 2018). However, our study sites
404 are on a coast undergoing a rapid transgression which may be driving imbalances between substrate supply and
405 microbial abundances. The rates of methane production observed at RP and TP of up to 154 nmol cm⁻³ d⁻¹ contrast
406 with reported values for methylotrophic methanogenesis (Maltby et al., 2018). Based on these numbers,
407 noncompetitive substrates likely play a small role in the total methane production at our study sites but further
408 investigation into methylotrophic methane production in coastal environments will allow to document the overall role
409 of methylotrophic methane production in coastal permafrost settings.

410 (2) Syntrophic methanogenesis occurs when molecular hydrogen produced by acetoclastic sulfate-reducing
411 bacteria is used by hydrogenotrophic methanogens. In this syntrophy, the chemical energy is shared via interspecies
412 hydrogen transfer (Ozuolmez et al., 2015). For instance, in permafrost soils of Sweden, it was demonstrated that
413 syntrophic methanogenesis was favored in anoxic and water-saturated soils by an elevated abundance in methanogens
414 and their syntrophic partners (Keuschnig et al., 2022). As the incubation experiment in our study at RP and TP featured
415 water-saturated and anoxic environments, syntrophic methanogenesis could participate in the co-occurrence of sulfate-
416 reduction and methanogenesis. This mechanism is consistent with most incubations producing methane with a $\delta^{13}\text{C}$
417 value in the range of hydrogenotrophic methanogenesis (see below).

418 Measuring methane production through incubations inherently has limitations as they prevent continuous inputs of
419 microorganisms, fresh OM and nutrients that would occur in the natural environment. This can create a “bottle effect”,
420 which leads to restrictions in microbial community composition, limits the input of nutrients and leads to the
421 accumulation of metabolites which would normally be degraded (Ionescu et al., 2015). Typically, overestimation of
422 microbial processes rates is observed compared to *in situ* data (Sherr et al., 1999). The overestimation of CH₄
423 production rates by incubations relative to the *in situ* rates are difficult to assess because of a lack of data in permafrost
424 environments (Heslop et al., 2020). Furthermore, a lag time between the start of anaerobic incubations and maximum
425 CH₄ production rate is widely documented, which appears to be the case for both active layer and thawed permafrost
426 incubations (Holm et al., 2020; Knoblauch et al., 2018; Knoblauch et al., 2013; Roy Chowdry et al., 2015). Drier or
427 water-unsaturated conditions lead to a longer lag time before the onset of maximum CH₄ production (Treat et al.,
428 2015). The long duration of our incubations (339 days), combined with the absence of substrate monitoring, may have
429 influenced the calculated production rates. While environmental conditions were fixed after the transition from *in situ*
430 to incubation settings, internal changes such as substrate depletion, accumulation of metabolic byproducts, and shifts
431 in microbial community composition likely occurred over time. These processes may have altered methanogenic

432 activity relative to initial conditions, particularly as more labile organic matter may have become depleted. Such
433 temporal dynamics are inherent to long-term incubation experiments and may lead to deviations from *in situ* rates.

434 Microbial community composition in the soil or sediment also exerts a strong control on the organic carbon
435 degradation and has been shown to change throughout the incubations (Holm et al., 2020). Low initial methanogen
436 population in soils can contribute to this lag time, but other factors such as disturbance of sediment during sampling,
437 substrate availability and redox state can also contribute to the observed lag time in some incubations (Treat et al.,
438 2015; Roy Chowdry et al., 2015).

439 Furthermore, it is also possible that a “priming effect” from the addition of brackish water in incubations could
440 have supercharged OM degradation with marine organic carbon, nutrients and microorganisms (Bianchi, 2011), which
441 may have enhanced CH₄ production. However, this priming effect was not observed in the Harbor sediments which
442 were amended with the same brackish water. Furthermore, CH₄ ebullition samples collected from pondlets adjacent
443 to RP and TP exhibited broadly similar $\delta^{13}\text{C}$ values to methane produced in incubations (Fig 6), suggesting a similitude
444 in microbial degradation pathways to methane *in situ* and in the incubations. Despite these uncertainties, our dataset
445 shows clear depth trends and landscape-level variations, indicating that even under brackish water addition, local
446 conditions will strongly influence CH₄ production.

447 **4.2 CH₄ production pathways depend on hydrology and organic matter lability**

448 The addition of brackish water resulted in incubation conditions being water-saturated in all cases, but it
449 appears that biological and hydrological conditions of the polygonal patterned grounds influenced the magnitude of
450 CH₄ production, nonetheless.

451 In all landforms, CH₄ production rates were lower at the inland site, RP than at TP, the coastal site (Fig 4).
452 Inland, low-centered polygons and troughs have typically higher CH₄ fluxes than unsaturated landforms like high-
453 centered polygons (Roy Chowdry et al., 2015; Martin et al., 2018; Zheng et al., 2018) which indicates they may also
454 have higher CH₄ production rates. Within sites in our study, brackish water amended incubations of high-centered
455 polygon soils had lower CH₄ production rates, while brackish water amended incubations of troughs and low-centered
456 polygons had higher CH₄ production rates (Fig 4). This suggests that under brackish water addition, CH₄ production
457 can still occur in tundra soils, increasing seawater interactions through coastal processes, such as submersion due to
458 subsidence or increased storm severity, resulting in the input of seawater in terrestrial soils, does not prevent
459 CH₄ production under the conditions tested, although the extent to which sulfate may suppress methanogenesis relative
460 to baseline conditions cannot be assessed. It also shows that landforms and local hydrology remain important in
461 controlling the microbial communities which likely influences the resulting CH₄ production. Differences among
462 landforms and sites are generally large and clearly exceed the range of variability as shown by the uncertainty ,
463 supporting the use of means with standard deviations to convey contrasts without formal statistical tests. This approach
464 allows us to highlight pronounced differences in methane production potential and geochemical context across coastal
465 and inland sites.

466 Marine OM and nutrient inputs from tides and storm surges may contribute to the higher lability of OM and
467 could fuel greater fermentation (Valdemarsen and Kristensen, 2010). It was reported that 8.7% of the organic carbon
468 in nearshore sediments of Herschel Island, Beaufort Sea, came from marine sources (Couture et al., 2018). This is
469 relevant for the TP site because while $\delta^{13}\text{C}$ signature of soils showed that terrestrial OM is dominant (Fig S6), marine
470 OM may get transported and deposited in coastal soils during high tides and storm surges. Although our analyses
471 could not detect the presence of marine OM in TP soils, the higher CH_4 production rates recorded in the incubations
472 of TP, relatively to those of RP could in part be explained by marine OM and nutrient inputs. Interestingly, the high-
473 centered polygon at TP, profile 09 (Fig 4), did not behave in a predictable manner, since it had very high CH_4
474 production rates on the surface. This elevated methane production rate coincided with the presence of substantial
475 goose fecal deposits at TP, profile 09. While this observation suggests a potential local input of labile organic matter
476 and nutrients (e.g., N and P) and possibly a distinct surface microbial community, no direct measurements were
477 conducted to establish a mechanistic link. This site-specific observation is therefore reported as contextual field
478 information rather than evidence of causation. Lower in the profile, CH_4 production rates were very low, characteristic
479 of the CH_4 production rates observed in water-unsaturated high-centered polygons (Fig 4). Therefore, in this instance,
480 proximity with the coast may have influenced CH_4 production through the presence of fauna.

481 Stable carbon isotopic signature of CH_4 provides insights on the microbial processes involved in
482 methanogenesis and on substrates used. $\delta^{13}\text{C}\text{-CH}_4$ between -65‰ and -50‰ is typically associated with acetoclastic
483 methanogenesis, while $\delta^{13}\text{C}\text{-CH}_4$ between -110‰ and -60‰ is associated with hydrogenotrophic methanogenesis
484 (Hornibrook et al., 1997, 2000). The stable isotopic signature of methylotrophic methanogenesis is between -83‰ and
485 -72‰ (Penger et al., 2012), which overlaps with the hydrogenotrophic interval, precluding us from separating these
486 two metabolic pathways. At RP, except for profile 10B, $\delta^{13}\text{C}\text{-CH}_4$ had more negative values, consistent with
487 hydrogenotrophic methanogenesis, which is often associated with the degradation of more recalcitrant organic matter
488 (Heffernan et al., 2022; Hodgkins et al., 2014). Profile 10B, a polygonal trough, had less negative $^{13}\text{C}\text{-CH}_4$ values
489 more consistent with acetoclastic methanogenesis (Hornibrook et al., 1997). At TP, the coastal polygonal tundra, δ
490 $^{13}\text{C}\text{-CH}_4$ at 5 cm depth is less negative, consistent with methanogenesis with more labile organic carbon and the
491 acetoclastic production pathway (Hodgkins et al., 2014), transitioning to more negative values, associated to
492 hydrogenotrophic production with depth. This shift suggests an input of labile OM in TP surface and sub-surface soils.
493 This may be due to the labile OM from abundant geese fecal matter that was observed in the surface. It is also possible
494 that *Carex sp.*, the dominant plant species of the site, may be a source of labile fermentation precursors (Galand et al.,
495 2010; Liebner et al., 2015). To evaluate whether $\delta^{13}\text{C}\text{-CH}_4$ covaried with other geochemical properties measured in
496 this study, $\delta^{13}\text{C}\text{-CH}_4$ values were examined alongside TOC content and sulfate concentrations; however, no consistent
497 relationships were observed across landforms or depths (Fig. S4), indicating that methanogenic pathway signatures
498 are not straightforwardly predicted by bulk TOC or sulfate availability at the scale investigated. Given the limited
499 number of isotopic measurements and biological replicates, these interpretations should be considered preliminary
500 and reflective of dominant trends rather than definitive pathway partitioning. It is also clear that future work should

501 integrate measurements of organic matter degradation, microbial community composition, and pore water chemistry
502 to better resolve the mechanisms driving spatial variability in methane production.

503 **4.3 Total CH₄ production rates are comparable to the net CH₄ fluxes measured in similar environments**

504 In a polygonal terrain of the Tuktoyaktuk Coastlands, net CH₄ fluxes from the center of high-centered polygons
505 and troughs derived from flux chambers were measured to be 1.9 ± 20.4 mmol m⁻² d⁻¹ and 13.0 ± 20.4 mmol m⁻² d⁻¹
506 respectively (Martin et al., 2018). These overlap with values of estimated total CH₄ production derived from the
507 brackish water amended incubation experiments (Fig. 5). It is clear from the large variations in measured CH₄
508 emissions from the study of Martin et al., (2018) that incubations to estimate total active layer CH₄ production rates
509 can discern small differences due to local variations that stem mostly from the polygonal features. For example, at
510 RP a comparable polygonal terrain located in the same study area of Martin et al., (2018), the total CH₄ production of
511 high-centered polygons and trough were 0.3 ± 0.1 mmol m⁻² d⁻¹ and 5.0 ± 2.0 mmol m⁻² d⁻¹ (Fig. 5), respectively which
512 are significantly different. This supports the idea that polygonal forms play an important role in controlling the activity
513 of microbial communities which controls CH₄ production and the potential to scale more accurately CH₄ production
514 at the landscape level based on landform distributions.

515 Interestingly, TP, the coastal site, had an estimated total CH₄ production rate comparable to emissions of a St.
516 Lawrence estuary salt marsh which had a CH₄ flux of 24 ± 14.4 mmol m⁻² d⁻¹ (Comer-Warner et al., 2022). The St.
517 Lawrence estuary salt marshes are affected by freeze-thaw cycles associated with seasons comparable to the freeze-
518 thaw cycles observed in the active layer of Tuktoyaktuk coastlands despite lacking some characteristics features of
519 our site like the presence of permafrost and rapid coastal erosion rates. CH₄ emissions and production within areas of
520 coastal influence thus appear of similar magnitude. By comparison, mangrove forests, which are a major global source
521 of CH₄ but a very different environment from coastal Arctic polygon terrain, had average CH₄ fluxes to the atmosphere
522 of 0.3 ± 0.1 mmol m⁻² d⁻¹ (Rosentreter et al., 2018). In another study, the average measured CH₄ flux from a Yangtze
523 Estuary (China) tidal salt marsh, with a subtropical monsoon climate, was 2.4 mmol m⁻² d⁻¹ (Li et al., 2021). These
524 reported values are similar to our study as well as other studies in the region. When considered alongside the global
525 distribution of coastal wetlands, this similarity in flux magnitude becomes particularly relevant. Tropical coastal
526 wetlands are dominated by mangroves (~147,000 km²), whereas Arctic wetlands cover approximately 3.5 million km²
527 (Worthington et al., 2024). Even if only a small fraction of Arctic wetlands is located within coastal zones, their total
528 extent is comparable to the global mangrove area (Worthington et al., 2024), suggesting that permafrost Arctic coastal
529 wetlands could potentially represent a non-negligible component of the global CH₄ budget and warrant further
530 investigation.

531 The calculated total methane production rates (T) from TP and RP do not take into account aerobic and anaerobic
532 oxidation of CH₄, which will most likely reduce fluxes of CH₄ from these sites. Studies and models of Arctic soils
533 emissions have highlighted that aerobic methanotrophy could consume more than half of the CH₄ produced in soils,
534 greatly limiting surface emissions (Oh et al., 2020; Zheng et al., 2018). Furthermore, AOM has been shown to play
535 an important role in attenuating CH₄ production in soils and sediments (Segarra et al., 2013; Winkel et al., 2019) but

536 did not appear to influence significantly CH₄ production in incubations with thermokarst lake sediments (Lotem et al.,
 537 2023). While AOM represents a major sink for CH₄ in marine sediments (Knittel and Boetius, 2009; Reeburgh, 2007),
 538 the very different biogeochemical and hydrological characteristics of our coastal sites suggest that the role of AOM
 539 in these environments may diverge from that observed in fully marine systems. Recent work in coastal thermokarst
 540 lagoons, which can present key similarities to our coastal study sites due to episodic or persistent brackish water
 541 intrusion, have been shown to exhibit strong AOM control on CH₄ dynamics, particularly in sulfate-rich settings where
 542 AOM may constitute a major CH₄ sink (Yang et al., 2023). For the discussion of this study, we compared results of
 543 brackish water incubations to CH₄ emissions measured in other landscapes. Such comparisons provide valuable
 544 context by comparing long-term microbial production processes with net atmospheric fluxes. However, we emphasize
 545 that CH₄ production rates cannot be directly equated to CH₄ emissions.

546

547 **Table 1.** Total methane production in a context of brackish water addition in high-centered polygons, low-centered
 548 polygons and troughs during growing season applied to the spatial scale of the polygonal landscape of RP. Two
 549 samples were taken for the high-centered polygon. The mean active layer and talik depth of the region is 35 cm. The
 550 error represents the propagation of the analytical uncertainty from the incubations results.

Geomorphological form	Relative area of each landform (km ²)	Estimated Total CH ₄ production (mol d ⁻¹)
High-centered polygons	0.0803	20.7 ± 10.3
Low-centered polygons	0.119	284 ± 123
Troughs	0.0362	182 ± 73.4

551

552 To better frame the potential impact of brackish water addition at scale, we extrapolated its consequence to a 25
 553 hectare area of polygonal tundra surrounding RP (Fig S2). This estimate simulates CH₄ production following the
 554 infiltration of brackish water into the terrestrial polygonal landscape around Tuktoyaktuk. This event could result from
 555 coastal flooding during storm surges, which are frequent in the Mackenzie River delta (Kokelj et al., 2012; Solomon
 556 et al., 2005). Taking into consideration the distribution of the polygonal features within RP and the relative areas of
 557 each landform, the CH₄ production rates in the active layer, excluding pondlets, for an area of 25 ha was estimated to
 558 be 487 mol d⁻¹ (Table 1) or 22 nmol m⁻² s⁻¹ and is consistent with the CH₄ emissions measured from various wetland
 559 types (Cui et al., 2024). The increasing sensitivity of wetlands to climate change and the preponderant role of carbon
 560 substrate availability in controlling global methane emissions (Hu et al., 2024) warrants further investigating CH₄
 561 dynamics in thawing continuous permafrost landscapes and the role of coastal processes influencing these emissions.
 562 More polygonal tundra in various settings should be investigated as a comparison to the studied region. Further
 563 research on aerobic and anaerobic CH₄ oxidation is necessary to provide a more precise estimate of the CH₄ cycle

564 inputs and outputs in a scope of the evaluation of its impacts on the greenhouse gas feedback loop. This extrapolation
565 is based on a limited number of sampled profiles per landform and should therefore be interpreted as a first-order
566 estimate intended to illustrate potential magnitudes rather than a precise landscape-scale quantification.

567 **5 Conclusions**

568 The primary hypothesis for this study was that an increase in waterlogged environments due to coastal
569 flooding and inundation processes would not enhance CH₄ production because of sulfate present in coastal waters.
570 While the extent to which sulfate may suppress methanogenesis relative to baseline conditions cannot be assessed, our
571 incubation experiments revealed that CH₄ production can occur at high rates in the presence of sulfate under brackish
572 water addition. . Additionally, waterlogged conditions attributed to the ebb and flow of tides, seems to favor anoxic
573 OM degradation and may potentially provide inputs of fresh OM and nutrients from marine sources, contributing to
574 the elevated CH₄ production rates measured in the coastal setting of TP. Moreover, no conclusive mechanism for the
575 apparent co-occurrence of sulfate reduction and methanogenesis in our incubations was identified, although syntrophic
576 methanogenesis may contribute. While these findings provide insight into methane production under brackish water
577 influence, the limited number of sampled profiles and replication for certain measurements warrant caution when
578 extending these results to broader landscape scales. Furthermore, more investigation on methylotrophic
579 methanogenesis in coastal soils are needed as it can be an important process in saline environments (Conrad, 2020).
580 Future studies should investigate CH₄ oxidation processes in greater detail, as they could provide crucial insights into
581 Arctic coastal carbon cycling in sediments and soils affected by changing sea level.

582 **Data availability**

583 All raw data of incubation experiment and other analyses performed and generated by study are available as
584 supplementary information.

585 **Competing interests**

586 The authors declare that they have no conflict of interest.

587 **Author contributions**

588 AP designed the experiment; ARL executed the experiments and analyses. AP, ARL, DW, RL participated in the
589 fieldwork. PMJD provided lab space, equipment and insights for the stable carbon isotopes analyses on incubation
590 CH₄. RL performed all GIS analyses and maps. ARL performed the data interpretation and generated all figures. AP
591 provided expertise on the writing and interpretation of figures. All authors reviewed and edited the manuscript.

592 **Acknowledgements**

593 We thank Santiago Mareque for assistance during field sampling. Mathieu Babin and Thi Hao Bui are acknowledged
594 for assisting with the laboratory work performed at Université du Québec à Rimouski and at McGill University,
595 respectively. Takuvik Laboratory is acknowledged for providing analyses and results on $\delta^{13}\text{C}$ and TOC content of

596 sediments. We also thank the community of Tuktoyaktuk for providing wildlife monitors with insightful information
597 on the territory during field sampling. This research was funded by NSERC Discovery Grant and Northern Supplement
598 to AP. ARL acknowledges financial support from the NSERC Northern Scientific Training Program. PMJD
599 acknowledges support from the NSERC Discovery Grant and the Canadian Foundation for Innovation.

600 **Financial support**

601 Support funds and grant agreement numbers are listed as specified upon manuscript registration.

602 **References**

603 AMAP: AMAP Climate Change Update 2019: An Update to Key Findings of Snow, Water, Ice and Permafrost in the
604 Arctic (SWIPA) 2017, Arctic Monitoring and Assessment Programme (AMAP), Oslo, Norway, 12 pp., 2019.

605 AMAP: Snow, Water, Ice and Permafrost in the Arctic (SWIPA) 2017, Arctic Monitoring and Assessment Programme
606 (AMAP), Oslo, Norway, xiv + 269 pp., 2017.

607 Andrachuk, M. and Smit, B.: Community-based vulnerability assessment of Tuktoyaktuk, NWT, Canada to
608 environmental and socio-economic changes, *Regional Environmental Change*, 12, 867–
609 885, <https://doi.org/10.1007/s10113-012-0299-0>, 2012.

610 Bianchi, T. S.: The role of terrestrially derived organic carbon in the coastal ocean: A changing paradigm and the
611 priming effect, *Proceedings of the National Academy of Sciences*, 108, 19473–
612 19481, <https://doi.org/10.1073/pnas.1017982108>, 2011.

613 Boetius, A., Ravenschlag, K., Schubert, C. J., Rickert, D., Widdel, F., Gieseke, A., Amann, R., Jørgensen, B. B.,
614 Witte, U., and Pfannkuche, O.: A marine microbial consortium apparently mediating anaerobic oxidation of
615 methane, *Nature*, 407, 623–626, <https://doi.org/10.1038/35036572>, 2000.

616 Comer-Warner, S. A., Ullah, S., Ampuero Reyes, W., Krause, S., and Chmura, G. L.: *Spartina alterniflora* has the
617 highest methane emissions in a St. Lawrence estuary salt marsh, *Environmental Research: Ecology*, 1,
618 011003, <https://doi.org/10.1088/2752-664X/ac706a>, 2022.

619 Conrad, R.: Importance of hydrogenotrophic, acetoclastic and methylotrophic methanogenesis for methane production
620 in terrestrial, aquatic and other anoxic environments: A mini review, *Pedosphere*, 30, 25–
621 39, [https://doi.org/10.1016/S1002-0160\(18\)60052-9](https://doi.org/10.1016/S1002-0160(18)60052-9), 2020.

622 Coolen, M. J. L. and Orsi, W. D.: The transcriptional response of microbial communities in thawing Alaskan
623 permafrost soils, *Frontiers in Microbiology*, 6, 197, <https://doi.org/10.3389/fmicb.2015.00197>, 2015.

624 Costa, B.: Remote sensing analysis of recent coastal change and controlling factors in Tuktoyaktuk Peninsula
625 (Beaufort Sea Coast, Canada), Master's dissertation, University of Lisbon, Repository of Lisbon University,
626 2022.

627 Couture, N. J., Irrgang, A., Pollard, W., Lantuit, H., and Fritz, M.: Coastal erosion of permafrost soils along the Yukon
628 Coastal Plain and fluxes of organic carbon to the Canadian Beaufort Sea, *Journal of Geophysical Research:*
629 *Biogeosciences*, 123, 406–422, <https://doi.org/10.1002/2017JG004166>, 2018.

- 630 Cui, S., Liu, P., Guo, H., Nielsen, C. K., Pullens, J. W. M., Chen, Q., Pugliese, L., and Wu, S.: Wetland hydrological
631 dynamics and methane emissions, *Communications Earth and Environment*, 5,
632 1635, <https://doi.org/10.1038/s43247-024-01635-w>, 2024.
- 633 Bridgman, S. D., Cadillo-Quiroz, H., Keller, J. K., and Zhuang, Q.: Methane emissions from wetlands:
634 biogeochemical, microbial, and modeling perspectives from local to global scales, *Global Change Biology*, 19,
635 1325–1346, <https://doi.org/10.1111/gcb.12131>, 2012.
- 636 Dallimore, S. R., Wolfe, S. A., Matthews Jr., J. V., and Vincent, J.-S.: Mid-Wisconsinan eolian deposits of the
637 Kittigazuit Formation, Tuktoyaktuk Coastlands, Northwest Territories, Canada, *Canadian Journal of Earth
638 Sciences*, 34, 1421–1441, <https://doi.org/10.1139/e17-116>, 1997.
- 639 Elberling, B., Michelsen, A., Schädel, C., Schuur, E. A. G., Christiansen, H. H., Berg, L., Tamstorf, M. P., and
640 Sigsgaard, C.: Long-term CO₂ production following permafrost thaw, *Nature Climate Change*, 3, 890–
641 894, <https://doi.org/10.1038/nclimate1955>, 2013.
- 642 Froelich, P., Klinkhammer, G., Bender, M., Luedtke, N., Heath, G., Cullen, D., Dauphin, P., Hammond, D., Hartman,
643 B., and Maynard, V.: Early oxidation of organic matter in pelagic sediments of the eastern equatorial Atlantic:
644 suboxic diagenesis, *Geochimica et Cosmochimica Acta*, 43, 1075–1090, [https://doi.org/10.1016/0016-
645 7037\(79\)90095-4](https://doi.org/10.1016/0016-7037(79)90095-4), 1979.
- 646 Fu, Q. A., Boutton, T. W., Ehleringer, J. R., and Flagler, R. B.: Environmental and developmental effects on carbon
647 isotope discrimination by two species of *Phaseolus*, in: *Stable Isotopes and Plant Carbon-Water Relations*,
648 Elsevier, 297–309, <https://doi.org/10.1016/B978-0-08-091801-3.50028-3>, 1993.
- 649 Galand, P. E., Yrjälä, K., and Conrad, R.: Stable carbon isotope fractionation during methanogenesis in three boreal
650 peatland ecosystems, *Biogeosciences*, 7, 3893–3900, <https://doi.org/10.5194/bg-7-3893-2010>, 2010.
- 651 Guimond, J. A., Mohammed, A. A., Walvoord, M. A., Bense, V. F., and Kurylyk, B. L.: Saltwater intrusion intensifies
652 coastal permafrost thaw, *Geophysical Research Letters*, 48,
653 e2021GL094776, <https://doi.org/10.1029/2021GL094776>, 2021.
- 654 Heffernan, L., Cavaco, M. A., Bhatia, M. P., Estop-Aragonés, C., Knorr, K.-H., and Olefeldt, D.: High peatland
655 methane emissions following permafrost thaw: enhanced acetoclastic methanogenesis during early
656 successional stages, *Biogeosciences*, 19, 3051–3071, <https://doi.org/10.5194/bg-19-3051-2022>, 2022.
657
- 658 Heslop, J. K., Walter Anthony, K. M., Sepulveda-Jauregui, A., Martinez-Cruz, K., Bondurant, A., Grosse, G., and
659 Jones, M. C.: Thermokarst lake methanogenesis along a complete talik profile, *Biogeosciences*, 12,
660 4317–4331, <https://doi.org/10.5194/bg-12-4317-2015>, 2015.
661
- 662 Heslop, J. K., Walter Anthony, K. M., Winkel, M., Sepulveda-Jauregui, A., Martinez-Cruz, K., Bondurant, A., Grosse,
663 G., and Liebner, S.: A synthesis of methane dynamics in thermokarst lake environments, *Earth-Science Reviews*,
664 210, 103365, <https://doi.org/10.1016/j.earscirev.2020.103365>, 2020.
- 665 Heyer, J., Berger, U., Kuzin, I. L., and Yakovlev, O. N.: Methane emissions from different ecosystem structures of
666 the subarctic tundra in Western Siberia during midsummer and during the thawing period, *Tellus B*, 54, 231–
667 249, <https://doi.org/10.1034/j.1600-0889.2002.01280.x>, 2002.
- 668 Hill, P. R., Héquette, A., and Ruz, M.-H.: Holocene sea-level history of the Canadian Beaufort shelf, *Canadian Journal
669 of Earth Sciences*, 30, 103–108, <https://doi.org/10.1139/e93-009>, 1993.

- 670 Hodgkins, S. B., Tfaily, M. M., McCalley, C. K., Logan, T. A., Crill, P. M., Saleska, S. R., Rich, V. I., and Chanton,
671 J. P.: Changes in peat chemistry associated with permafrost thaw increase greenhouse gas production,
672 Proceedings of the National Academy of Sciences, 111, 5819–5824, <https://doi.org/10.1073/pnas.1314641111>,
673 2014.
- 674 Holm, S., Walz, J., Horn, F., Yang, S., Grigoriev, M. N., Wagner, D., Knoblauch, C., and Liebner, S.: Methanogenic
675 response to long-term permafrost thaw is determined by paleoenvironment, FEMS Microbiology Ecology, 96,
676 fiaa021, <https://doi.org/10.1093/femsec/fiaa021>, 2020.
- 677 Hornibrook, E. R. C., Longstaffe, F. J., and Fyfe, W. S.: Evolution of stable carbon isotope compositions for methane
678 and carbon dioxide in freshwater wetlands and other anaerobic environments, Geochimica et Cosmochimica
679 Acta, 64, 1013–1027, [https://doi.org/10.1016/S0016-7037\(99\)00321-X](https://doi.org/10.1016/S0016-7037(99)00321-X), 2000.
- 680 Hornibrook, E. R., Longstaffe, F. J., and Fyfe, W. S.: Spatial distribution of microbial methane production pathways
681 in temperate zone wetland soils: stable carbon and hydrogen isotope evidence, Geochimica et Cosmochimica
682 Acta, 61, 745–753, [https://doi.org/10.1016/S0016-7037\(96\)00368-7](https://doi.org/10.1016/S0016-7037(96)00368-7), 1997.
- 683 Hu, H., Chen, J., Zhou, F., Nie, M., Hou, D., Liu, H., Delgado-Baquerizo, M., Ni, H., Huang, W., Zhou, J., Song, X.,
684 Cao, X., Sun, B., Zhang, J., Crowther, T. W., and Liang, Y.: Relative increases in CH₄ and CO₂ emissions from
685 wetlands under global warming dependent on soil carbon substrates, Nature Geoscience, 17, 26–
686 31, <https://doi.org/10.1038/s41561-023-01345-6>, 2024.
- 687 Hu, K., Issler, D., Chen, Z., and Brent, T.: Permafrost investigation by well logs, and seismic velocity and repeated
688 shallow temperature surveys, Beaufort-Mackenzie Basin, Geological Survey of
689 Canada, <https://doi.org/10.4095/293120>, 2013.
- 690 Hynes, S., Solomon, S. M., and Whalen, D.: GIS compilation of coastline variability spanning 60 years in the
691 Mackenzie Delta and Tuktoyaktuk in the Beaufort Sea, Geological Survey of Canada Open File
692 7685, <https://doi.org/10.4095/295579>, 2014.
- 693 Ionescu, D., Bizic-Ionescu, M., Khalili, A., Malekmohammadi, R., Morad, M. R., de Beer, D., and Grossart, H.-P.:
694 A new tool for long-term studies of POM-bacteria interactions: overcoming the century-old Bottle Effect,
695 Scientific Reports, 5, 14706, <https://doi.org/10.1038/srep14706>, 2015.
- 696 Irrgang, A. M., Bendixen, M., Farquharson, L. M., Baranskaya, A. V., Erikson, L. H., Gibbs, A. E., Ogorodov, S.
697 A., Overduin, P. P., Lantuit, H., Grigoriev, M. N., and Jones, B. M.: Drivers, dynamics and impacts of
698 changing Arctic coasts, Nature Reviews Earth and Environment, 3, 39–54, [https://doi.org/10.1038/s43017-
699 021-00232-1](https://doi.org/10.1038/s43017-021-00232-1), 2022.
- 700 Jenrich, M., Wolter, J., Liebner, S., Knoblauch, C., Grosse, G., Giebler, F., Whalen, D., and Strauss, J.: Rising Arctic
701 seas and thawing permafrost: uncovering the carbon cycle impact in a thermokarst lagoon system in the outer
702 Mackenzie Delta, Canada, Biogeosciences, 22, 2069–2086, <https://doi.org/10.5194/bg-22-2069-2025>, 2025.
- 703 Jenrich, M., Angelopoulos, M., Liebner, S., Treat, C. C., Knoblauch, C., Yang, S., Grosse, G., Giebler, F., Jongejans,
704 L. L., Grigoriev, M., and Strauss, J.: Greenhouse gas production and microbial response during the transition
705 from terrestrial permafrost to a marine environment, Permafrost and Periglacial Processes, published online 4
706 October 2024, <https://doi.org/10.1002/ppp.2251>, 2024.

- 707 Jones, E. L., Hodson, A. J., Thornton, S. F., Redeker, K. R., Rogers, J., Wynn, P. M., Dixon, T. J., Bottrell, S. H., and
708 O'Neill, H. B.: Biogeochemical processes in the active layer and permafrost of a high Arctic fjord valley,
709 *Frontiers in Earth Science*, 8, 342, <https://doi.org/10.3389/feart.2020.00342>, 2020.
- 710 Keuschnig, C., Larose, C., Rudner, M., Pesqueda, A., Doleac, S., Elberling, B., Björk, R. G., Klemetsson, L., and
711 Björkman, M. P.: Reduced methane emissions in former permafrost soils driven by vegetation and microbial
712 changes following drainage, *Global Change Biology*, 28, 3411–3425, <https://doi.org/10.1111/gcb.16137>, 2022.
- 713 Knittel, K. and Boetius, A.: Anaerobic oxidation of methane: progress with an unknown process, *Annual Review of*
714 *Microbiology*, 63, 311–334, <https://doi.org/10.1146/annurev.micro.61.080706.093130>, 2009.
- 715 Knoblauch, C., Beer, C., Liebner, S., Grigoriev, M. N., and Pfeiffer, E.-M.: Methane production as key to the
716 greenhouse gas budget of thawing permafrost, *Nature Climate Change*, 8, 309–
717 312, <https://doi.org/10.1038/s41558-018-0095-z>, 2018.
- 718 Knoblauch, C., Beer, C., Sosnin, A., Wagner, D., and Pfeiffer, E.-M.: Predicting long-term carbon mineralization and
719 trace gas production from thawing permafrost of Northeast Siberia, *Global Change Biology*, 19, 1160–
720 1172, <https://doi.org/10.1111/gcb.12116>, 2013.
- 721 Kokelj, S. V., Lantz, T. C., Solomon, S., Pisaric, M. F., Keith, D., Morse, P., Thienpont, J. R., Smol, J. P., and Esagok,
722 D.: Using multiple sources of knowledge to investigate northern environmental change: regional ecological
723 impacts of a storm surge in the Outer Mackenzie Delta, N.W.T., *Arctic*, 65,
724 3, <https://doi.org/10.14430/arctic4214>, 2012.
- 725 Kramshøj, M., Albers, C. N., Holst, T., Holzinger, R., Elberling, B., and Rinnan, R.: Biogenic volatile release from
726 permafrost thaw is determined by the soil microbial sink, *Nature Communications*, 9,
727 3412, <https://doi.org/10.1038/s41467-018-05824-y>, 2018.
- 728 Kroeger, K. D., Crooks, S., Moseman-Valtierra, S., and Tang, J.: Restoring tides to reduce methane emissions in
729 impounded wetlands: a new and potent blue carbon climate change intervention, *Scientific Reports*, 7,
730 12138, <https://doi.org/10.1038/s41598-017-12138-4>, 2017.
- 731 La, W., Han, X., Liu, C.-Q., Ding, H., Liu, M., Sun, F., Li, S., and Lang, Y.: Sulfate concentrations affect sulfate
732 reduction pathways and methane consumption in coastal wetlands, *Water Research*, 217,
733 118441, <https://doi.org/10.1016/j.watres.2022.118441>, 2022.
- 734 Lacelle, D., Fontaine, M., Pellerin, A., Kokelj, S. V., and Clark, I. D.: Legacy of Holocene landscape changes on soil
735 biogeochemistry: a perspective from paleo-active layers in northwestern Canada, *Journal of Geophysical*
736 *Research: Biogeosciences*, 124, 2662–2679, <https://doi.org/10.1029/2018JG004916>, 2019.
- 737 Lantuit, H., Overduin, P. P., Couture, N., Wetterich, S., Aré, F., Atkinson, D., Brown, J., Cherkashov, G., Drozdov,
738 D., Forbes, D. L., Graves-Gaylord, A., Grigoriev, M., Hubberten, H.-W., Jordan, J., Jorgenson, T., Ødegård, R.
739 S., Ogorodov, S., Pollard, W. H., Rachold, V., and Vasiliev, A.: The Arctic coastal dynamics database: a new
740 classification scheme and statistics on Arctic permafrost coastlines, *Estuaries and Coasts*, 35, 383–
741 400, <https://doi.org/10.1007/s12237-010-9362-6>, 2012.
- 742 Lapham, L. L., Dallimore, S. R., Magen, C., Henderson, L. C., Powers, L. C., Gonsior, M., Clark, B., Côté, M., Fraser,
743 P., and Orcutt, B. N.: Microbial greenhouse gas dynamics associated with warming coastal permafrost, western
744 Canadian Arctic, *Frontiers in Earth Science*, 8, 582103, <https://doi.org/10.3389/feart.2020.582103>, 2020.
- 745 Li, Y., Wang, D., Chen, Z., Chen, J., Hu, H., and Wang, R.: Methane emissions during the tide cycle of a Yangtze
746 Estuary salt marsh, *Atmosphere*, 12, 245, <https://doi.org/10.3390/atmos12020245>, 2021.

- 747 Liebner, S., Ganzert, L., Kiss, A., Yang, S., Wagner, D., and Svenning, M. M.: Shifts in methanogenic community
748 composition and methane fluxes along the degradation of discontinuous permafrost, *Frontiers in Microbiology*,
749 6, 356, <https://doi.org/10.3389/fmicb.2015.00356>, 2015.
- 750 Lim, M., Whalen, D., Martin, J., Mann, P. J., Hayes, S., Fraser, P., Berry, H. B., and Ouellette, D.: Massive ice control
751 on permafrost coast erosion and sensitivity, *Geophysical Research Letters*, 47,
752 e2020GL087917, <https://doi.org/10.1029/2020GL087917>, 2020.
- 753 Lipson, D. A., Zona, D., Raab, T. K., Bozzolo, F., Mauritz, M., and Oechel, W. C.: Water-table height and
754 microtopography control biogeochemical cycling in an Arctic coastal tundra ecosystem, *Biogeosciences*, 9,
755 577–591, <https://doi.org/10.5194/bg-9-577-2012>, 2012.
- 756 Lotem, N., Pellerin, A., Anthony, K. W., Gafni, A., Boyko, V., and Sivan, O.: Anaerobic oxidation of methane does
757 not attenuate methane emissions from thermokarst lakes, *Limnology and Oceanography*, 68, 1316–
758 1330, <https://doi.org/10.1002/lno.12349>, 2023.
- 759 Lovley, D. R. and Klug, M. J.: Sulfate reducers can outcompete methanogens at freshwater sulfate concentrations,
760 *Applied and Environmental Microbiology*, 45, 187–192, <https://doi.org/10.1128/aem.45.1.187-192.1983>, 1983.
- 761 Mackay, J. R. and Dallimore, S. R.: Massive ice of the Tuktoyaktuk area, western Arctic coast, Canada, *Canadian*
762 *Journal of Earth Sciences*, 29, 1235–1249, <https://doi.org/10.1139/e92-099>, 1992.
- 763 Maltby, J., Steinle, L., Löscher, C. R., Bange, H. W., Fischer, M. A., Schmidt, M., and Treude, T.: Microbial
764 methanogenesis in the sulfate-reducing zone of sediments in the Eckernförde Bay, SW Baltic Sea,
765 *Biogeosciences*, 15, 137–157, <https://doi.org/10.5194/bg-15-137-2018>, 2018.
- 766 Martens, C. S. and Berner, R. A.: Methane production in the interstitial waters of sulfate-depleted marine sediments,
767 *Science*, 185, 1167–1169, <https://doi.org/10.1126/science.185.4157.1167>, 1974.
- 768 Martin, A. F., Lantz, T. C., and Humphreys, E. R.: Ice wedge degradation and CO₂ and CH₄ emissions in the
769 Tuktoyaktuk Coastlands, Northwest Territories, *Arctic Science*, 4, 130–145, <https://doi.org/10.1139/as-2016-0011>, 2018.
- 771 Manson, G. K., Couture, N. J., and James, T. S.: CanCoast 2.0: data and indices to describe the sensitivity of Canada's
772 marine coasts to changing climate, *Geological Survey of Canada Open File*
773 8551, <https://doi.org/10.4095/314669>, 2019.
- 774 Murton, J. B.: Thermokarst-lake-basin sediments, Tuktoyaktuk Coastlands, western Arctic Canada, *Sedimentology*,
775 43, 737–760, <https://doi.org/10.1111/j.1365-3091.1996.tb02023.x>, 1996.
- 776 Oh, Y., Zhuang, Q., Liu, L., Welp, L. R., Lau, M. C. Y., Onstott, T. C., Medvigy, D., Bruhwiler, L., Dlugokencky, E.
777 J., Hugelius, G., D'Imperio, L., and Elberling, B.: Reduced net methane emissions due to microbial methane
778 oxidation in a warmer Arctic, *Nature Climate Change*, 10, 317–321, [https://doi.org/10.1038/s41558-020-0734-](https://doi.org/10.1038/s41558-020-0734-z)
779 z, 2020.
- 780 Oremland, R. S. and Polcin, S.: Methanogenesis and sulfate reduction: competitive and noncompetitive substrates in
781 estuarine sediments, *Applied and Environmental Microbiology*, 44, 1270–
782 1276, <https://doi.org/10.1128/aem.44.6.1270-1276.1982>, 1982.
- 783 Ozuolmez, D., Na, H., Lever, M. A., Kjeldsen, K. U., Jørgensen, B. B., and Plugge, C. M.: Methanogenic archaea and
784 sulfate reducing bacteria co-cultured on acetate: teamwork or coexistence?, *Frontiers in Microbiology*, 6,
785 492, <https://doi.org/10.3389/fmicb.2015.00492>, 2015.

- 786 Pellerin, A., Lotem, N., Walter Anthony, K., Eliani Russak, E., Hasson, N., Røy, H., Chanton, J. P., and Sivan, O.:
787 Methane production controls in a young thermokarst lake formed by abrupt permafrost thaw, *Global Change*
788 *Biology*, 28, 3206–3221, <https://doi.org/10.1111/gcb.16151>, 2022.
- 789 Penger, J., Conrad, R., and Blaser, M.: Stable carbon isotope fractionation by methylotrophic methanogenic archaea,
790 *Applied and Environmental Microbiology*, 78, 7596–7602, <https://doi.org/10.1128/AEM.01773-12>, 2012.
- 791 Petersen, S. G. G., Kristensen, E., and Quintana, C. O.: Greenhouse gas emissions from agricultural land before and
792 after permanent flooding with seawater or freshwater, *Estuaries and Coasts*, 46, 1459–
793 1474, <https://doi.org/10.1007/s12237-023-01218-6>, 2023.
- 794 Poffenbarger, H. J., Needelman, B. A., and Megonigal, J. P.: Salinity influence on methane emissions from tidal
795 marshes, *Wetlands*, 31, 831–842, <https://doi.org/10.1007/s13157-011-0197-0>, 2011.
- 796 Pönisch, D. L., Breznikar, A., Gutekunst, C. N., Jurasinski, G., Voss, M., and Rehder, G.: Nutrient release and flux
797 dynamics of CO₂, CH₄, and N₂O in a coastal peatland driven by actively induced rewetting with brackish water
798 from the Baltic Sea, *Biogeosciences*, 20, 295–323, <https://doi.org/10.5194/bg-20-295-2023>, 2023.
- 799 Rampton, V. N.: Quaternary geology of the Tuktoyaktuk coastlands, Northwest Territories, Geological Survey of
800 Canada, 1988.
- 801 Reeburgh, W. S.: Oceanic methane biogeochemistry, *Chemical Reviews*, 107, 486–
802 513, <https://doi.org/10.1021/cr050362v>, 2009.
- 803 Rosentreter, J. A., Maher, D. T., Erler, D. V., Murray, R. H., and Eyre, B. D.: Methane emissions partially offset blue
804 carbon burial in mangroves, *Science Advances*, 4, eao4985, <https://doi.org/10.1126/sciadv.aao4985>, 2018.
- 805 Roy Chowdhury, T., Herndon, E. M., Phelps, T. J., Elias, D. A., Gu, B., Liang, L., Wullschleger, S. D., and Graham,
806 D. E.: Stoichiometry and temperature sensitivity of methanogenesis and CO₂ production from saturated
807 polygonal tundra in Barrow, Alaska, *Global Change Biology*, 21, 722–737, <https://doi.org/10.1111/gcb.12762>,
808 2015.
- 809 Schuur, E. A. G., McGuire, A. D., Schädel, C., Grosse, G., Harden, J. W., Hayes, D. J., Hugelius, G., Koven, C. D.,
810 Kuhry, P., Lawrence, D. M., Natali, S. M., Olefeldt, D., Romanovsky, V. E., Schaefer, K., Turetsky, M. R.,
811 Treat, C. C., and Vonk, J. E.: Climate change and the permafrost carbon feedback, *Nature*, 520, 171–
812 179, <https://doi.org/10.1038/nature14338>, 2015.
- 813 Segarra, K. E., Comerford, C., Slaughter, J., and Joye, S. B.: Impact of electron acceptor availability on the anaerobic
814 oxidation of methane in coastal freshwater and brackish wetland sediments, *Geochimica et Cosmochimica Acta*,
815 115, 15–30, <https://doi.org/10.1016/j.gca.2013.03.029>, 2013.
- 816 Sepulveda-Jauregui, A., Walter Anthony, K. M., Martinez-Cruz, K., Greene, S., and Thalasso, F.: Methane and carbon
817 dioxide emissions from 40 lakes along a north–south latitudinal transect in Alaska, *Biogeosciences*, 12, 3197–
818 3223, <https://doi.org/10.5194/bg-12-3197-2015>, 2015.
- 819 Sela-Adler, M., Ronen, Z., Herut, B., Antler, G., Vigderovich, H., Eckert, W., and Sivan, O.: Co-existence of
820 methanogenesis and sulfate reduction with common substrates in sulfate-rich estuarine sediments, *Frontiers in*
821 *Microbiology*, 8, 766, <https://doi.org/10.3389/fmicb.2017.00766>, 2017.
- 822 Sherr, E., Sherr, B., and Sigmon, C.: Activity of marine bacteria under incubated and in situ conditions, *Aquatic*
823 *Microbial Ecology*, 20, 213–223, <https://doi.org/10.3354/ame020213>, 1999.

- 824 Skoog, D. A., West, D. M., Holler, F. J., and Crouch, S. R.: Fundamentals of analytical chemistry, 9th ed., Cengage
825 Learning, Singapore, 2014.
- 826 Solomon, S. M., Whalen, D., Saper, R., and Mulvie, J.: Measuring the extent of storm surge flooding on the Mackenzie
827 River Delta, Northwest Territories, Canada using synthetic aperture radar, in: Proceedings of the 8th
828 International Conference on Remote Sensing for Marine and Coastal Environments, 2005.
- 829 Vardy, S. R., Warner, B. G., and Aravena, R.: Holocene climate effects on the development of a peatland on the
830 Tuktoyaktuk Peninsula, Northwest Territories, Quaternary Research, 47, 90–
831 104, <https://doi.org/10.1006/qres.1996.1869>, 1997.
- 832 Vaughn, L. J. S., Conrad, M. E., Bill, M., and Torn, M. S.: Isotopic insights into methane production, oxidation, and
833 emissions in Arctic polygon tundra, Global Change Biology, 22, 3487–3502, <https://doi.org/10.1111/gcb.13281>,
834 2016.
- 835 Steedman, A. E., Lantz, T. C., and Kokelj, S. V.: Spatio-temporal variation in high-centre polygons and ice-wedge
836 melt ponds, Tuktoyaktuk Coastlands, Northwest Territories, Permafrost and Periglacial Processes, 28, 66–
837 78, <https://doi.org/10.1002/ppp.1880>, 2017.
- 838 Tanski, G., Bröder, L., Wagner, D., Knoblauch, C., Lantuit, H., Beer, C., Sachs, T., Fritz, M., Tesi, T., Koch, B. P.,
839 Haghypour, N., Eglinton, T. I., Strauss, J., and Vonk, J. E.: Permafrost carbon and CO₂ pathways differ at
840 contrasting coastal erosion sites in the Canadian Arctic, Frontiers in Earth Science, 9,
841 630493, <https://doi.org/10.3389/feart.2021.630493>, 2021.
- 842 Richter, T., Šantrůčková, H., Schädel, C., Schuur, E. A. G., Sloan, V. L., Turetsky, M. R., and Waldrop, M. P.: A pan-
843 Arctic synthesis of CH₄ and CO₂ production from anoxic soil incubations, Global Change Biology, 21, 2787–
844 2803, <https://doi.org/10.1111/gcb.12875>, 2015.
- 845 Treat, C. C., Wollheim, W. M., Varner, R. K., Grandy, A. S., Talbot, J., and Frolking, S.: Temperature and peat type
846 control CO₂ and CH₄ production in Alaskan permafrost peats, Global Change Biology, 20, 2674–
847 2686, <https://doi.org/10.1111/gcb.12572>, 2014.
- 848 Turetsky, M. R., Treat, C. C., Waldrop, M. P., Waddington, J. M., Harden, J. W., and McGuire, A. D.: Short-term
849 response of methane fluxes and methanogen activity to water table and soil warming manipulations in an
850 Alaskan peatland, Journal of Geophysical Research: Biogeosciences, 113,
851 G03S05, <https://doi.org/10.1029/2007JG000496>, 2008.
- 852 Valdemarsen, T. B. and Kristensen, E.: Degradation of dissolved organic monomers and short-chain fatty acids in
853 sandy marine sediment by fermentation and sulfate reduction, Geochimica et Cosmochimica Acta, 74, 1593–
854 1605, <https://doi.org/10.1016/j.gca.2009.12.009>, 2010.
- 855 Whalen, D., Forbes, D. L., Kostylev, V., Lim, M., Fraser, P., Nedimović, M. R., and Stuckey, S.: Mechanisms,
856 volumetric assessment, and prognosis for rapid coastal erosion of Tuktoyaktuk Island, an important natural
857 barrier for the harbour and community, Canadian Journal of Earth Sciences, 59, 945–
858 960, <https://doi.org/10.1139/cjes-2021-0101>, 2022.
- 859 Winfrey, M. R. and Ward, D. M.: Substrates for sulfate reduction and methane production in intertidal sediments,
860 Applied and Environmental Microbiology, 45, 193–199, <https://doi.org/10.1128/aem.45.1.193-199.1983>, 1983.
- 861 Winkel, M., Sepulveda-Jauregui, A., Martinez-Cruz, K., Heslop, J. K., Rijkers, R., Horn, F., Liebner, S., and Walter
862 Anthony, K. M.: First evidence for cold-adapted anaerobic oxidation of methane in deep sediments of

- 863 thermokarst lakes, *Environmental Research Communications*, 1, 021002, <https://doi.org/10.1088/2515-7620/ab1042>, 2019.
- 864
- 865 Yang, S., Anthony, S. E., Jenrich, M., in 't Zandt, M. H., Strauss, J., Overduin, P. P., Grosse, G., Angelopoulos, M.,
866 Biskaborn, B. K., Grigoriev, M. N., Wagner, D., Knoblauch, C., Jaeschke, A., Rethemeyer, J., and Liebner, S.:
867 Microbial methane cycling in sediments of Arctic thermokarst lagoons, *Global Change Biology*, 29, 2714–
868 2731, <https://doi.org/10.1111/gcb.16649>, 2023.
- 869 Ye, R., Keller, J. K., Jin, Q., Bohannan, B. J., and Bridgham, S. D.: Peatland types influence the inhibitory effects of
870 a humic substance analog on methane production, *Geoderma*, 265, 131–
871 140, <https://doi.org/10.1016/j.geoderma.2015.11.026>, 2016.
- 872 Yuan, J., Liu, D., Ji, Y., Xiang, J., Lin, Y., Wu, M., and Ding, W.: *Spartina alterniflora* invasion drastically increases
873 methane production potential by shifting methanogenesis from hydrogenotrophic to methylotrophic pathway in
874 a coastal marsh, *Journal of Ecology*, 107, 2436–2450, <https://doi.org/10.1111/1365-2745.13164>, 2019.
- 875 Zheng, J., RoyChowdhury, T., Yang, Z., Gu, B., Wullschleger, S. D., and Graham, D. E.: Impacts of temperature and
876 soil characteristics on methane production and oxidation in Arctic tundra, *Biogeosciences*, 15, 6621–
877 6635, <https://doi.org/10.5194/bg-15-6621-2018>, 2018.